Investigation of the Effects of Humidity and Surface Charge on Partial Discharge in Insulator Posts Under DC Voltage

by

Haoliang Deng

A Thesis submitted to the Faculty of Graduate Studies of
The University of Manitoba
in partial fulfilment of the requirements of the degree of

Master of Science

Department of Electrical and Computer Engineering
University of Manitoba
Winnipeg, Canada

Examining Committee

This thesis was examined and approved by the following examining committee on March 6, 2020:

- **Dr. B. Kordi** (advisor)

  Department of Electrical & Computer Engineering

  University of Manitoba

- **Dr. A. Rajapakse**

  Department of Electrical & Computer Engineering

  University of Manitoba

- **Dr. N. Fernando**

  Department of Electrical & Computer Engineering

  University of Manitoba

Abstract

The flashover mechanism and performance of insulators have always been significant of importance to insulation engineers' attention. A serious flashover accident will damage insulators and influence the reliability of the whole converter station and result in severe outages. It is believed that the flashover and partial discharge phenomena are strongly related to environmental conditions such as temperature, humidity, pressure, pollution's, and even space charges. The motivation of this thesis was to study the random discharge phenomenon that was observed in a Manitoba Hydro's HVDC substation to avoid further insulation damages. However, the lack of data prevents engineers from making firm conclusions. As such a data acquisition system was proposed that will collect leakage current data flowing in a reactor's insulation post, to help to build a better understanding of the correlation between PD and environmental influences.

The field tests at the HVDC substation studied the behavior of the leakage current from smoothing reactor's ground wire and its associated electric field changes. Through the field tests, we found that the discharge phenomena exists only under certain weather conditions were. One hypothesis for partial discharge occurring on the insulator stacks is the influences of moisture and static charge. Moisture helps the static charge buildup on the insulator will spread along the insulator surface and create a conducting path between the smoothing reactor, flange, and ground. The sharp edge of the flange within this conducting path will generate corona and cause a discharge problem.

For the laboratory experiments, humidity and surface charge studies were implemented in air

and on FRP insulators under HVDC in order to get a better understanding of environmental influences on partial discharge behaviors. The results demonstrated that for a given electrode configuration, both humidity and surface charge have significant effects on the behavior of partial discharge. We also noticed that the relationship between total charge magnitude Q and equivalent frequency F followed a curve with exponential decay, and under high humidity environment or with surface charge present, the decay speed was faster than normal conditions. And the lab results also proved that time-frequency-charge (TFQ) mapping technique can be used for HVDC PD identifications.

Acknowledgements

First, I would like to express many thanks to my advisor Dr. Behzad Kordi for his guidance and patience through my M.Sc. His brilliant advice and support during my studies have encouraged me to keep going. I would also like to express my gratitude to Adam Hayward for providing this great opportunity and for his exceptional suggestions throughout my thesis. His passion for his job is a wonderful encouragement for young engineers and scientists. I am also thankful to the examiners of my thesis, Prof. Rajapakse and Dr. Fernando, for their time and contribution examining this thesis.

I am also grateful to Daryl Hamelin, Cory Smit, and Zoran Trajkoski for their kind help and practical knowledge when solving problems during the thesis at the laboratory.

Financial support from faculty of graduate studies and Manitoba Hydro is gratefully acknowledged. Last, but definitely not least, I would like to thank my family and friends. Many sincere thanks to my loving parents, Hongzhi Deng and Lizhen Chen, for their kindness, patience, and support while I was pursuing my studies away from them. Without my parents' encouragement, I would have never been able to follow my dreams.

Dedication

To my lovely, supportive mother and father,

to whom who believes in justice and fights for a world with more justice,

to whom who dares to explore and goes beyond the limits.

Table of Contents

List of Figures

Chapter 1

Introduction

1.1 Background and Motivation

When it comes to power transmission over long distances, High Voltage Direct Current (HVDC) transmission becomes the first choice for utilities. With the increase of DC voltage levels, the challenges for system studies and equipment manufacturers have become a hot topic around the world [1]. As a very important piece of equipment in HVDC substations, smoothing reactors are designed to decrease harmonic voltages and currents in the DC line. They also can protect DC converters from steep voltages by smoothing the ripple in the DC current that was generated in DC transmission lines or switches [2]. Since air-cored smoothing reactors are cheaper and lighter than oil insulated reactors, they are employed in many HVDC projects [1]. In a project that occurred between 2010 and 2013, Manitoba Hydro procured and installed air-cooled-air-cored coils to function as DC smoothing reactors at converter stations. Each coil was supported by 6 insulator posts and each post consisted of two insulators which made by high strength aluminous porcelain follows C130-IEC60672-3 Standard. The reactors were energized at nominal voltages between +/-450kV and +/-500kV. During operation, it was noted that the insulator columns exhibited visible corona discharge at various locations along their vertical length, especially at the connection

flange especially during certain weather conditions. The occurrence of discharge is irregular and intermittent, and the root cause of the effect is not well known.

The motivation of this research was local unusual discharge phenomenon that was observed in a Manitoba Hydro's HVDC substation that needs to be better understood and considered when testing and designing HVDC insulation systems. Manitoba Hydro believes the uncertainty of this abnormal discharge phenomena might be a latent danger to cause serious flashover which will damage insulators. Thus, this issue will lead to a reliability problem of the whole converter station and may result in severe outages. Further, the flashover mechanism and performance of insulators have always been significant of importance to insulation engineers' attention. It is believed that the flashover and partial discharge phenomena are strongly related to environmental conditions such as temperature, humidity, pressure, pollution's, and even space charges. Due to the mechanism of DC, HVDC system can trap significant amount of free charge around it. However, the lack of data prevents engineers from making firm conclusions.

Monitor partial discharge, as a symptom of insulation deterioration can be used to improve the reliability of HV insulation. Usually, the techniques employed for PD detection are based on chemical [3], acoustic [4], optical [5] and electrical which all involved with ultra frequency measurements. The electrical measurement of PD in HVDC systems are widely used and are the focus of this thesis. In general, a ultra frequency data acquisition system was proposed that will collect leakage current data flowing in a reactor's insulation post, to help to build a better understanding of the correlation between PD and environmental influences. If the visible discharge is caused by environmental influences, it is important to get a better understanding of the environmental influences and take serious consideration for future HVDC insulation systems design. Further, this research project can help Manitoba Hydro to reduce the risk of a flashover/fault, avoid further insulation damage caused, and improve the reliability of the HVDC substation.

1.2 Objective of the Thesis

The main objective of this M.Sc thesis is to study the correlation between the partial discharge and humidity and surface free charges influences at HVDC substation. The hypothesis is the contribution of moisture and surface charge stack around the insulator reduce the partial discharge inception voltage and causes corona and visible arcs. Based on this hypothesis, in this research, I designed and developed a robust, low-cost sensing system for monitoring the leakage currents from the surface of the insulators. This system aims at collecting insulator surface leakage current, electrical field near the insulator post and local environmental information (temperature, humidity, and pressure) for further data analysis. Signal processing techniques like: fast fourier transform (FFT), continuous wavelet transform (CWT), short time fourier transform (STFT) were implemented for segmented signal frequency analysis. The signal processing result helped us discovered that corona discharge happened at HVDC substation are related to local weather conditions.

To test the hypothesis regarding the correlation between PD behaviours and environment influences, laboratory experiments setups to model HVDC partial discharge in different insulation media and environment were designed. Obtaining accurate and reliable measurements to study HVDC partial discharge was the most important properties of this research. To start analyzing the measured data, signal were recorded and implemented with appropriate signal processing algorithm (wavelet, TFQ maps) under different conditions, then auto-correlation and K-means cluster were used for further analysis and classification. In this way, the result of laboratory experiments were able to build a correlation between the HVDC partial discharge and environmental influences. The results of this research can aid help utilities that operate or plan the insulation system in the HVDC substation especially design the insulation on smoothing reactors. Further, the proposed leakage current monitor system can be used on any project that requires recording and analysis of small high-frequency signals. Benefits to the scientific and engineering discipline will include a better understanding of the correlation between PD and environmental influences.

1.3 Methodology and Contributions

This M.Sc thesis presents an insulator leakage current monitor system that will investigate the relationship between the HVDC partial discharge and environment influences. The proposed study methodology consists of field studies and laboratory experiments prove. The field tests at the HVDC substation studied the behaviour of the leakage current from smoothing reactor's ground wire and its associated electric field changes. Based on the analysis results of the signals from field tests, we were able to create a scaled model in high voltage lab for further HVDC partial discharge behavior under the influence of humidity and surface charge. Once the current and electrical field signals are segmented recorded, different methods of noise reduction are employed to extract features of each PD signal. Then different PD source identification algorithm are implemented on processed signal to study the environmental influences by analysing the changes of extracted features of PD pulses.

This M.Sc thesis contributes in the areas of:

- A robust, low-cost sensing system are designed and proposed for monitoring the leakage currents over the surface of the insulators at HVDC substation. The system consists two Rogowski coils, one electrical field sensor, one weather environmental sensor, and one wind speed sensor. The proposed system were implement in the HVDC substation and proved its ability to identify partial discharge signal at noisy environment. This capability enables online monitoring of high voltage insulation more accurately and efficiently which helps to avoid further insulation damage and improve the reliability of the substation .

- Fast fourier transform (FFT), continuous wavelet transform (CWT), short time fourier transform (STFT) were implemented on field tests signals for frequency analysis. The results demonstrated that captured leakage current can be separated into a periodic signal and random partial discharge pulses.

- PSACD 12 pulses HVDC Transmission System Cigre Benchmark model were employed to study the voltage across the smoothing reactors. The result shows that the periodic leakage current's

frequency matches the frequency of voltage across the reactor, which means there is great chance the periodic leakage current is generated by the switching behavior of DC valves.

- Rogowski coils and parallel plate electric field sensor are been proved to be efficient and reliable for partial discharge detection. Due to their costs and flexibility, these sensors can be widely used in industry partial discharge detection.

- Test sets were designed to study HVDC partial discharge behaviours under different environment influences. The results demonstrated that for a given electrode configuration, both humidity and surface charge have significant effects on the behaviour of partial discharge.

- Equivalent time and frequency mapping technique is proposed for HVDC partial discharge identification. The reliability of this approach has been proved and will be considerably perceived dealing with HVDC partial discharge performance in high voltage insulation.

1.4 Thesis Outline

This thesis is classified into 5 chapters as defined below:

Chapter 1: Introduction, background information, problem definition and existing solutions, objectives, and contributions.

Chapter 2: Literature review of this study completed on partial discharge(PD),PD source identification (includes signal source and multiple active source), partial discharge characteristic under HVDC stress, and some common partial discharge signal processing techniques which will be used during this project.

Chapter 3: Discussion of the methodology and results of our three field partial-discharge tests on HVDC substation. Based on the signal processing result, we believe that the discharge phenomenon on the DC insulator is related to static charge buildup on the surface and environment humidity. Thus, we proposed a downscale lab model to simulate a similar situation and prove our hypothesis.

Chapter 4: Discussion on the methodology of the partial discharge's PDIV and flashover voltage tests under humid environmental conditions or with surface charges presents.

Chapter 5: Discussion of the lab results regarding the influence of surface charge and humidity on corona under HVDC conditions, proving the hypothesis discussed in Chapter 3.

Chapter 6: Conclusion of this thesis project, with a discussion of future work.

Chapter 2

Background and Literature Review

2.1 Partial Discharge (PD)

Based on the IEC60270 standard, partial discharge is defined as "localized electrical discharge that only partially bridges the insulation between conductors and which can or cannot occur adjacent to a conductor," [6]. The IEC60270 standard also states that:

> "Partial discharges are in general a consequence of local electrical stress concentrations in the insulation or on the surface of the insulation. Generally, such discharges appear as pulses having a duration of much less than 1 us. More continuous forms can, however, occur, such as the so-called pulseless discharges in gaseous dielectrics. Partial discharges are often accompanied by the emission of sound, light, heat, and chemical reactions," [6].

The importance of PD is because it will compromise insulation materials in both physical and chemical ways. If PD issues keep happening, it might eventually cause high-voltage equipment failure. Thus, detecting and mitigating PD problems is a critical topic in the field of high-voltage engineering. Based on different characteristics, PDs can be defined as internal discharge, surface discharge, and corona. By internal discharge it is meant that the discharges occur inside the solid insulation or at the edges of conductors in solid/liquid insulation. Surface discharge is a type of discharge that may occur on the surface of insulation material. Corona charge refers to partial discharge in

gasses around conductors that are removed from solid or liquid insulation. Partial discharge is a complex physical process with stochastic properties [24]. Some phenomena such as light, charge displacement, and acoustic noise are often observed when partial discharge occurs. Therefore, these phenomena might be used for detecting partial discharges sources. Based on the characteristics (physical and chemical) of PD's accompanied phenomena, most of PD detection techniques rely on chemical, acoustic, optical, electrical, and ultra high frequency (UHF) measurements. Before more details are discussed, some important definitions are presented as follows.

- Partial Discharge Pulse (PD pulse): In IEC 60270 standard, PD pulse is defined as a "current or voltage pulse that results from a partial discharge occurring within the object under test. The pulse is measured using suitable detector circuits, which have been introduced into the test circuit for the purpose of the test" [6].

- Discharge Inception Voltage (PDIV): "The inception voltage is the lowest applied voltage at which the magnitude of a PD pulse quantity becomes equal to or exceeds a specified low value" [6].

- Discharge Extinction Voltage (PDEV): "The extinction voltage U_e is the lowest applied voltage at which the magnitude of a chosen PD pulse quantity becomes equal to, or less than, a specified low value" [6].

- Apparent Charge (q): "Apparent charge q of a PD pulse is that charge which, if injected within a very short time between the terminals of the test object in a specified test circuit, would give the same reading on the measuring instrument as the PD current pulse itself. The apparent charge is usually expressed in pico-coulombs (pC). The apparent charge is not equal to the amount of charge locally involved at the site of the discharge, which cannot be measured directly" [6].

- PD Pulse Repetition Rate (n): "The ratio between the total number of PD pulses recorded in a selected time interval and the duration of this time interval. In practice, only pulses above a specified magnitude or within a specified range of magnitudes are considered" [6] .

2.2 Environmental Influences on Partial Discharge

The Manitoba Hydro isn't the only utility company with substation random partial discharge issues in the world. In 2014, Tony Byrne, a senior engineer consultant from EA Technology Limited, reported that some substations in Europe were facing insulation failure issues due to the high humidity level inside the stations [7]. In fact, the relationship between environmental conditions (including temperature, humidity, and space charge) and partial discharge performance has been the subject of considerable work by both physicists and engineers [8]. The following subsections will generally introduce how temperature, humidity, and space charge affect the behaviour of partial discharge.

2.2.1 Temperature

The temperature and temperature gradient across the insulation have major and complex influences on the PD behaviour [9]. These include the conductivity of dielectric and cavity change [9], redistribution of the electric field around the insulator [2,10,11], and affecting the relative humidity level changes [11–15].

In 2005, Morshuis and Smit proved that the resistances of dielectric and cavity are strongly affected by temperature [9]. Their tests showed that the conductivity of a dielectric changes by orders of magnitude when the temperature of the insulation is raised from an ambient temperature of $20°C$ to an operating temperature between $60°C$ and $90°C$. The PD repetition rate is directly affected by the increase in conductivity, meaning that an increase in conductivity by two orders of magnitude would result in a similar increase of the PD repetition rate [9]. In 2018, Guastavino showed that compared to the same PD source at ambient temperature of $23°C$, at $150°C$, the PD repetition rate became significantly higher [16]. Recently, Saadati, et al. published a paper regarding the fundamental difference of PD under AC and DC. By studying the PD characteristics generated by the cavity inside a insulation, they noticed that when the system was under HVDC stress, the PD repetition rate increases with the increment of temperature, until $60°C$. After $60°C$,

the PD repetition rate will slightly deceases due to a sudden voltage changes across the cavity [17]. They also provided a mathematical model to calculate the voltage over the cavity as:

$$V_{\mathrm{c}}(t) = \frac{R_{\mathrm{c}}}{R_{\mathrm{c}} + R_{\mathrm{b}}} V_{\mathrm{p}} \left(1 - e^{\frac{t}{\tau}}\right). \tag{2.1}$$

Here, R_c and R_b represent the resistance of the cavity and the resistance of dielectric borders [17]. The time constant τ is expressed as:

$$\tau = \frac{R_{\mathrm{b}} R_{\mathrm{c}} \left(C_{\mathrm{b}} + C_{\mathrm{c}}\right)}{R_{\mathrm{b}} + R_{\mathrm{c}}}. \tag{2.2}$$

Here, C_c and C_b present the capacitance of the cavity and the capacitance of dielectric borders [17]. By integrating temperature influences in Eq 2.1, they conclude that the time constant decreases rapidly with increasing temperature, and the faster recovery time leads to the increases of PD repetition rate [17, 18].

From an electric field effect perspective, a temperature gradient in the insulation will lead to a redistribution of the electric field which may lead to the disappearance of PD at some locations and the inception of PD at other locations [2, 10, 11]. This may especially affect the PD caused by a sharp edge, needle tip, and cavities [19–21]. In 2014, Mariut created a COMSOL model to study the electric field changes inside a micro-cavity due to thermal reaction. She states that as the temperature increases, the electric field inside the microcavity gets higher [19]. A number of researches have shown that high electric fields will cause free electrons, and they tend to be injected earlier from the PD sources [20, 21]. An earlier injected electron can lead to the drop of PDIV and an increase of PD repetition rate.

2.2.2 Humidity

Substantial research shows that humidity can affect partial discharge characteristics and lead to insulation failure if the situation becomes severe [22, 23]. It was found that the photoelectrons distribution within the ionization layer played an important role in deciding whether the inception voltage increased or decreased with relative humidity [11]. An important conclusion was that the corona inception voltage decreased with increasing relative humidity [8, 11, 24]. Back in 1991, Lemke, et al. performed a test to the study influences of air humidity on PD phenomena under DC stress. They assumed that the resistances of dust particles decreases with increasing the level of air humidity [25]. Therefore, micro-discharges may develop at highly humid environments due to the high-filed region around the dust particles [25]. This will also cause an increase in space charge generation [25, 26]. The increase of charge accumulation due to high humidity levels will lead to a reduction of PD intensity and cause a strong reduction of the PDIV [25, 27]. Another theory regarding the decease of PDIV due to high humidity levels was proposed by Abdel-Salam. Abdel-Salam proposed a mathematical model to calculate the corona inception voltage and corona current in humid air. The study shows that the thickness of the ionization zone around the insulator diminishes with the increase of humidity due to the increase of electron attachment coefficient η [11]. This will also slow down the decay speed of the emitted photons. Therefore, the growing avalanches in humid air are expected to have a higher eclectic field inside the ionization zone and cause the PDIV to decrease [11].

Abdel-Salam also proved that the effective ions' mobility decreases with the rise of relative humidity, so at high voltages, partial discharge leakage current decreases as the relative humidity rises [8, 11]. Abdel-Salam proposed that the ion mobility K_i in dry air $(K_i)_d$ equals [11]:

$$(K_{\mathrm{i}})_{\mathrm{d}} = K_0 \exp\left(-\frac{1}{\alpha}\int_{R_0}^{r}\frac{\mathrm{d}r}{E}\right), \tag{2.3}$$

where $a = 4 \times 10^{-6} m^2/V$ and K_0 is the ion mobility averaged over the ionization zone ($K_0 =$

$(4/1.8) \times 10^{-4} m^2 V^{-1} S^{-1}$). The ion mobility K_i in humid air is related to that in dry air as shown in (2.3), and that in water vapour $(K_i)_w$ as [11]:

$$\frac{1}{K_{\mathrm{i}}} = \frac{P_{\mathrm{w}}}{P\,(K_{\mathrm{i}})_{\mathrm{w}}} + \frac{P - P_{\mathrm{w}}}{P\,(K_{\mathrm{i}})_{\mathrm{d}}}, \tag{2.4}$$

where P_w is the partial pressure of water vapour and P is the air pressure in the precipitators. In 2013, Wang and You proved Abdel-Salam's theory and reported that the partial discharge current-voltage characteristics from the test unit were also significantly affected by the humidity [24]. It has been reported that the partial discharge pulse parameters were significantly affected by the humidity changes [24, 28]. In 2017, Lühring, et al. tested the influence of humidity on pulse shape parameters of PD under DC voltages. In their research, they found that the pulse's amplitude, width, rise time, and fall time rapidly reduced with increased relative humidity levels from 20% to 95% [28].

2.2.3 Surface Charge

Charges on the surface of insulators have also been found to strongly affect both the PDIV and flashover voltage [5, 29]. The accumulated charge attached on the surface of an insulator can increase the PD intensity and cause a significant reduction of the PDIV [25]. Moreover, Amer, et al. found that on certain electrode configurations, the flashover voltage is reduced when a positive charge is present on the insulator surface while it is conversely increased with a negative charge on the surface [5]. They used three different charging methods (energized needle ring, pre-stressing, and wiping), and all three tests showed that the surface charge affects the flashover voltage. When the system is energized, surface charge with the same polarity can cause flashover increments, and surface charge with different polarity can cause flashover reductions [5]. Takabayashi and Kubota also reported a similar phenomenon by using the rod to plane electrode configurations [29, 30] and proved that the PDIV also follows the same mechanism. The PDIV on the insulation sheet with the same polarity surface charge was larger than that without surface charge. On the other hand,

the PDIV on the paper insulation sheet with opposite polarity surface charge was lower [29].

Du and Xiao performed a study on the flashover impact of surface charge of flat Epoxy/BN Nano-composites under DC voltages [31]. With no surface charge, the negative flashover voltage was usually lower than positive polarity, but under surface charge influences, the results were close [5, 29, 30]. They concluded that the main reason for the decrease in flashover voltage was charge accumulation. By adding nanoparticles into the test system, they found that the introduced nanoparticles trapped charges and created accumulation which led to flashover voltage reduction [31].

Some computer simulation studies also proved that surface charges can affect flashover voltage. Kumara [32] proved that when the insulator is far from the ground, surface charges with positive polarity decrease the impulse flashover voltage (IFV), and negative surface charge increases IFV for both polarities of applied voltage. However, when the distance between the insulator and the ground gets closer, the result shows the opposite effects. For the positive IFV, surface charge with the same polarity causes an increase while negative charge causes a decrease. For negative IFV, both positive and negative surface charges cause a decrease in IFV, but positive charges only lead to a small difference [32].

2.3 Partial Discharge under DC Stress

Unlike AC systems, PD under DC voltage doesn't have phase information as a reference to establish the relationship between the source and signal characteristics [33]. Despite all the advancements, the PD source identification under DC voltage doesn't have a well-established standard. Many theories for the interpretation of PD under DC have been developed. However, none of them possesses the maturity which exists for related theories under AC voltage.

2.3.1 Measurement of Partial Discharge

Partial discharge are usually detected by integrating the displacement current magnitude, expressed in units of pC, in the ground leads of the test object [33]. Two critical conditions must be fulfilled to cause a discharge. Firstly, the electrical field at the location where the discharge starts, must exceed the minimal breakdown filed strength $E_{\min}$. Secondly, a starting electron must be present [33]. In Fromm's paper [33], three basic quantities related to the occurrence of a single discharge can be measured: the discharge magnitude q_i, the time of the discharge occurrence t_i, and the instantaneous voltage across the test object $V(t_i)$. For PD under DC, if the voltage $V(t_i)$ is known, the basic quantities can be reduced to the discharge magnitude q_i, the time of discharge occurrence t_i [33]. The discharge phenomena have a stochastic nature, so during the measurement, a large set of basic quantities can be recorded. It is important to reduce the large number of basic quantities to a few deduced quantities. At AC voltage, today there are several well-developed techniques like the $H(q^1, \varphi^2)$ histogram or the discharge q and phase angle φ from phase-resolved partial discharge (PRPD) patterns [33]. However, for DC voltage there is no generally accepted standard yet. Some popular techniques are the time function of discharge frequency and apparent discharge current, the distribution function of the discharge magnitude, equivalent time and frequency mapping system, and 3-dimensional $H(q, \Delta t_{\text{suc}}{}^3)$ distribution [33, 34].

2.4 PD Source Identification

Once partial discharges are detected and measured, the practical interest is to identify the source of the discharge and differentiate its pattern from that of any existing interference. In general, for the identification of partial discharge, two different types of PD patterns have been analyzed, namely, phase-resolved and time-resolved data [35]. In the phase resolved PD pattern, two important parameters, both about phase angles are discharge magnitude, and number count of discharges.

[1] q: discharge magnitude
[2] φ: phase angle of the discharge event
[3] Δt_{suc}: time to successive discharge

Time resolved data sets consist of discharge magnitudes in reference to the time [36]. To identify different sources of PD based on their patterns, signal processing and pattern recognition techniques are required to be employed. In the next two subsections, a review of the application of some pattern recognition and signal processing techniques that have been used in the last couple of decades for the identification of single and multi-source PDs is presented.

2.4.1 Single PD Source Identification

In the last three decades, automated recognition of single-source PD patterns has been progressively investigated and several signal processing methods and classification algorithms have been developed for analyzing single source discharge patterns. These include the relative identification factor [37], time series analysis [38], artificial neural networks [35], fuzzy algorithm [39], support vector machine [40], and K means [41]. The application of wavelet transforms has also been shown to be useful for PD source recognition [42, 43]. PD source classification requires a large database for training the engineers based on different PD test result. Almost all the tests were performed on artificial defects that implemented in controlled laboratory test cells [35–39, 41].

2.4.2 Multiple Simultaneously Active Source Identification

As mentioned, in the last three decades, automated recognition of PD patterns has been progressively studied and several PD classification algorithms have been applied to analyze discharge patterns [14, 35, 36, 44]. However, there are many practical situations where the interest lies in the identification of multiple, simultaneously activated PD sources in insulation. Recently, the identification of these types of defects has been receiving more attention [13, 45, 46]. To enhance a PD classification system, these multi-source PDs need to be successfully classified. However, PRPD patterns associated with multiple simultaneously activated PD sources are often partially overlapped [13, 47], making them very hard to appropriately classify using available methods in the literature. A few studies have been conducted in this regard, mainly based on analyzing the

PD pulse waveforms in several exploration ways (signal processing techniques) attempting to separate individual concurrent pulse sources [36] [48]. Classification of these types of multi-source PDs is subsequently performed on each selected single-source PD using its corresponding PRPD sub-patterns. This is usually done with the assumption that a relationship exists between the nature of PD sources and their generated pulse waveforms,one that helps distinguish different pulse waveforms originated from different sources [35–37, 44, 49] .

2.4.2.1 Auto-correlation and K-Means Clustering Technique

In 2009, Contin and Pastore proposed a PD signal classification and separation method by using auto-correlation and the K-Means clustering technique [41, 49]. The separation algorithm is based on the K-means classification (KMC) algorithm which categorizes a given set of signals into a certain number of groups. Signals are grouped around a representative signal by means of a distance measure. To prevent signals with similar shape but different energy from being classified to different groups, a normalized auto-correlation function (ACF) is adopted and applied to digital signals [41]. Assuming the measurement of PD signal returns N samples $\{S_1, S_2, ..., S_N\}$, each sample S_i is represented by a $2 \times N_C$ matrix $\{s_1, s_2, ..., s_{N_C};\ t_1, t_2, ..., t_{N_C}\}$, where s_i represents the voltage amplitude and t_i represents the signal's associate time stamp. The normalized auto-correlation function is given by [41]:

$$R_s[k] = \frac{\sum_{i=1}^{N_c} s(i)s(i+k)}{N_C} \frac{1}{E_s}, \tag{2.5}$$

where k is between 1 to N_C. E_S is the total energy of signal S as defined by [41]:

$$E_S = \frac{\sum_{i=1}^{N_C} s^2(i)}{N_C} \tag{2.6}$$

In this way, each ACF of the signal set is normalized with respect to energy, so the similarity between different ACFs depends only on the signal's shape [41]. Next correlation coefficient was

calculated to evaluate the similarity between two different profiles. For example: $R_1(k)$ and $R_2(k)$ are the ACF of the signal set S_1 and S_2. Let $\bar{R}_1$ and $\bar{R}_2$ be the mean and $var(R_1)$ and $var(R_2)$ be the variance of $R_1(k)$ and $R_2(k)$. The covariance, $\mathrm{cov}(R_1(k), R_2(k))$ is defined as [41]:

$$\mathrm{cov}\left(R_1, R_2\right) = \frac{\sum_{k=1}^{N_C}\left[R_1(k) - \bar{R}_1\right]\left[R_2(k) - \bar{R}_2\right]}{N_c - 1}. \tag{2.7}$$

The correlation index, ρ_c is [41]:

$$\rho_c = \frac{\mathrm{cov}\left(R_1, R_2\right)}{\sqrt{\mathrm{var}\left(R_1\right)}\sqrt{\mathrm{var}\left(R_2\right)}}, \tag{2.8}$$

where ρ_c is a real number between 0 an 1 since R(0) is always positive and normalized to unity 1. If two normalized auto-correlation functions (NACF) have the same shape and are completely correlated, ρ_c is 1, on the other hand, if they are completely uncorrelated, ρ_c is 0. In order to introduce a distance metric in NACF space, the chord distance, d_ρ has been adopted [41]:

$$d_\rho = \sqrt{2\left(1 - \rho_c\right)}. \tag{2.9}$$

If was found that a threshold level of $d_\rho < 0.4$ represents a good compromise between weak and strong discrimination. K-Means Clustering can be applied on pre-processed N samples of NACFs and move to the classification stage [41].

2.4.2.2 3-Dimensional $H(q, \Delta t_{\mathbf{suc}})$ Distribution

A histogram formed by basic parameters q and Δt_{suc} which described in section 2.3.1 can be used as a classification tool for DC partial discharge analysis. By study the distribution of $H(q, \Delta t_{\mathrm{suc}})$ histogram, trained engineer will be able to identify different PD sources in DC system.

The 3-dimensional $H(q, \Delta t_{suc})$ histogram has been found to be characteristic for specific types of discharges [33]. This means that the DC PD classification and recognition should be possible.

Based on the $H_q(\Delta t_{suc})$ histograms, an expert could visibly recognize some defects. For instance, in Figure 2.1, Fromm provides an example of corona in the air, a very narrow peak is the characteristic we should focus on [33]. For internal discharges, the maximum density is registered for the smallest measured discharge.

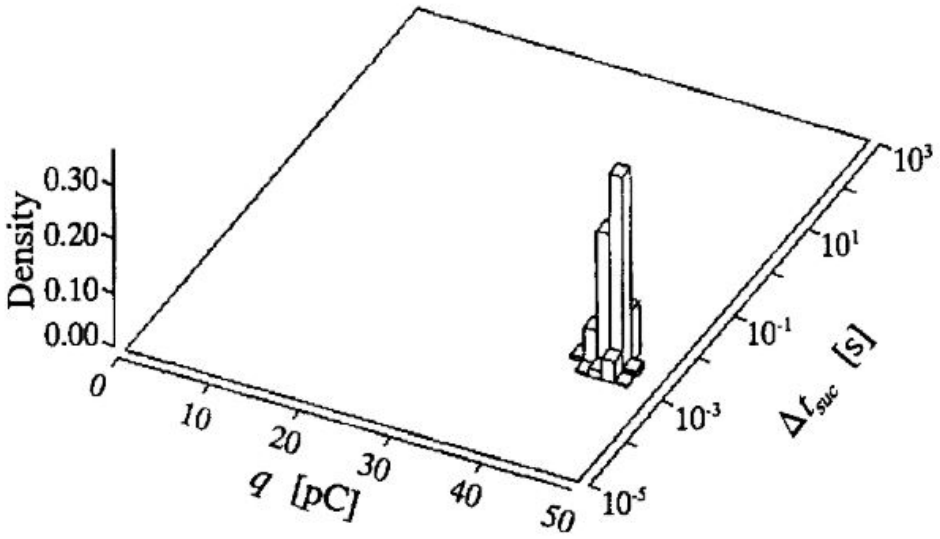

Fig. 2.1: $H(q, \Delta t_{\mathrm{suc}})$ histogram for corona in air at 8kV [33]

Based on Fromm's theory, more detailed 3-dimensional histogram were created to provide a precise mapping system to classify and recognize PD sources [33, 34, 50–52]. They are:

- $H_{\mathrm{q\ max}}(\Delta t_{\mathrm{pre}})$ and $H_{\mathrm{q\ max}}(\Delta t_{\mathrm{suc}})$, representing the maximum DC PD magnitude as a fuction of t_{pre} or t_{suc} .
- $H_{\mathrm{q\ n}}(\Delta t_{\mathrm{pre}})$ and $H_{\mathrm{q\ n}}(\Delta t_{\mathrm{suc}})$, representing the mean DC PD magnitude as a fuction of t_{pre} or t_{suc}.
- $H_{\mathrm{n}}(q)$ and $H_{\Sigma}(q)$, representing the discharge density and the cumulative discharge density.
- $H_n(\Delta t)$ and $H_{\Sigma}(\Delta t)$, representing the number and the cumulative number of pulses observed as

a function of Δt.

2.4.2.3 TF Mapping Model

Time-frequency (TF) mapping, also known as an equivalent time and frequency mapping technique, is one of the common tools for PD source identification under DC voltage [39,47,49]. In TF mapping, each waveform is composed of two quantities: equivalent duration and equivalent bandwidth. By locating these values on a two-dimensional plot, each waveform will convert to a point in the mapping system [47]. Scientists believe and have proven that different PD sources will have a unique position in this TF mapping system [42, 47, 49]. The definition of these parameters is expressed by:

$$T^2 = \frac{\sum_{i=1}^{k} (t_i - t_0)^2 \cdot s_i^2 (t_i)}{\sum_{i=1}^{k} s_i^2 (t_i)}, \tag{2.10}$$

where t_0 is,

$$t_0 = \frac{\sum_{i=1}^{k} t_i \cdot s_i^2 (t_i)}{\sum_{i=1}^{k} s_i^2 (t_i)}, \tag{2.11}$$

in which, k is the number of points in constituent waveforms, t_i is the i-th point over the pulse duration, s_i is the amplitude of the related signal that is i^{th} point in time, and t_0 is the average weight shown in (2.11).

And,

$$W^2 = \frac{\sum_{i=1}^{k} f_i^2 \cdot |X_i (f_i)|^2}{\sum_{i=1}^{k} |X_i (f_i)|^2}. \tag{2.12}$$

In (2.12), f_i is i^{th} sample point and $X_i(f)$ is the i^{th} component of the signal which is derived by the application of FFT transform.

The TF map is constructed by projecting the T^2 and W^2 of each PD pulse onto a two-dimensional plane. On this plane, the projected data points that belong to PD pulses with similar shape will form a distinct group. As a result, each formed group with similar PD characteristics will correspond to a unique PD source. This method provides a mechanism for describing an individual PD pulse in terms of time and frequency representations. However, even from the same PD source, PD pulses' shape cannot be always precisely represented since only overall amplitude/magnitude in the time/frequency domain of a PD pulse is considered [41]. As a consequence, sometimes the PD pulses from the same PD source can be clustered into different groups [42, 47]. In 2011, Hao introduced total charge Q of PD pulses into the TF map system to form the TFQ map system, that is a three-dimensional plot [42]. By introducing energy as the third principal component, Hao was able to improve the accuracy of PD source identification. In 2015, Chan proposed a TF sparsity map, which introduced sparsity values in decomposed signals and frequency domains [47]. The TF sparsity map can provide a more accurate result of PD pulses compared to the traditional TF map system by improving the accuracy of data clustering issues.

Chapter 3

Field Experimental Setup and Initial Data Analysis

Based on the description of partial discharge witness from Manitoba Hydro, we noticed that the corona noises and visible arcs were been reported only under specific conditions. A sample photo is shown in Figure 3.1 which is captured in 2013. The hypothesis that we need to answer is partial discharge activities at HVDC substation is affected by environmental factors. Thus, under certain environment conditions, the partial discharge will be more actively generated. Based on the literature reviews which described in the previous chapter, there is high possibility that the partial discharge impact factors are humidity and free surface charges.

To investigate the hypothesis, a leakage current and environmental monitoring system has been proposed for studying the relationship between PD activities and environmental influences. The details of the data acquisition system, field experimental setup, and data analysis results are presented and discussed in the following sections.

3.1 Data Acquisition System

The designed leakage current and environmental monitoring system requires multiple hardware components to operate. The system flow chart is shown in Figure 3.2 and depicts how the hardware components are utilized within the system. Further details of each hardware component can be

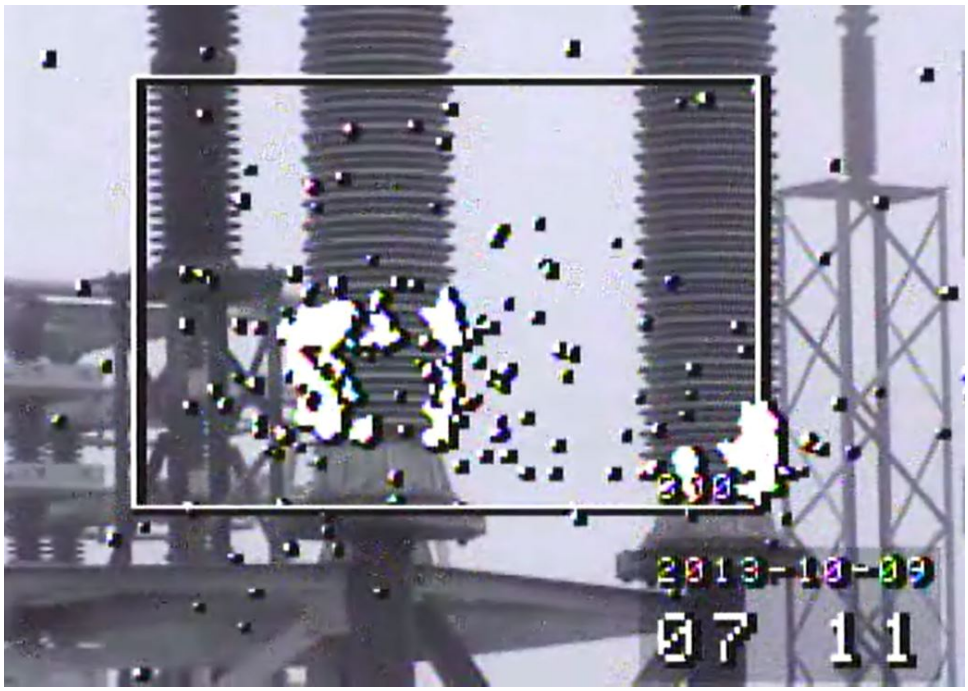

Fig. 3.1: PD activities captured by corona camera which happened only on the insulators close to flange.

found below.

The system consists of three major parts: a microcontroller unit (MCU), a high-speed analog to digital converter (ADC), and sensors (including two Rogowski coils, one electric field sensor, one environmental sensor for humidity and temperature, and one wind speed sensor). The purpose of this acquisition system is to accurately measure the leakage current from the smoothing reactor's insulation posts. By cross-checking the recorded current signal and related environmental information, we can establish a connection between discharge phenomena and environmental influences. Details of each piece of equipment in the system are displayed in Table 3.1 .

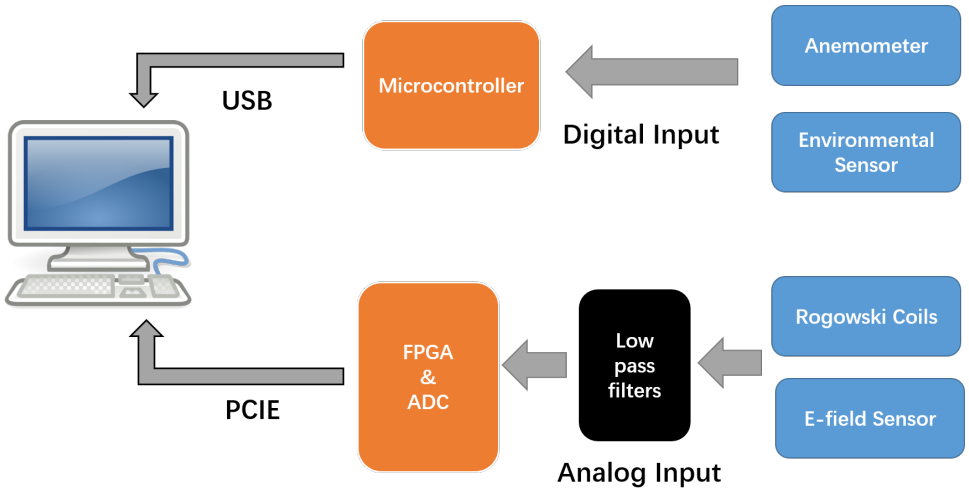

Fig. 3.2: Schematic of the data acquisition system flow diagram.

Table 3.1: Details of the data acquisition system design.

System Parts	Equipment's Detail
Microcontroller unit (MCU)	Texas Instruments C2000 Delfino MCUs F28377S
High-speed ADC unit	GaGe Octave 4 Channel 4 Channels @ 25 MS/s, 16-bit PCIe Digitizer
Current sensor	Customized Rogowski Coil with 20MHz bandwidth
Electric field sensor	Customized coupling capacitor (parallel plate antenna)
Environmental sensor	Bosch BME280
Anemometer	Davis Instruments Anemometer for Vantage Pro

3.2 HVDC Substation Field Experimental

Between September 2018 and March 2019, we visited the HVDC substation four times and did three field measurement tests on the smoothing reactor of the HVDC transmission line. During these three tests, we implemented our monitoring system in the HVDC substation to collect data. The monitoring system setup schematic is shown in Figure 3.3. The complete system setups at HVDC substation is shown in Figure 3.4 and 3.5.

Two specially-designed high-frequency Rogowski coils are mounted on the reactor's ground

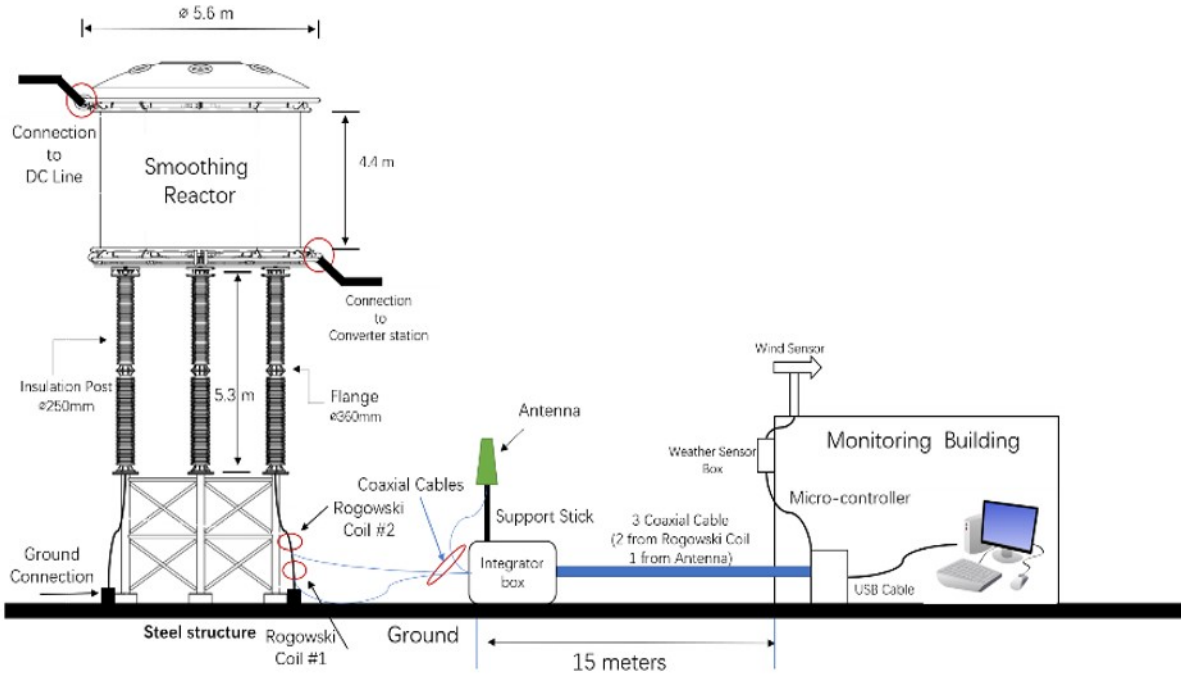

Fig. 3.3: Data acquisition system set-up at HVDC substation.

wire to collect leakage current from the insulator post. One Rogowski Coil is mounted at the top part of ground wire, while the other coil is mounted close to the ground. Each coil turns four times around the ground wire; the detailed setup is shown in Figure 3.4. The purpose of mounting both coils on the same ground wire is to analyze the direction of the detected current. By finding the current delay, we can find out whether the current goes from the top of the tower to the ground or the other way around.

An electric field sensor (parallel plate capacitor) is also mounted close to the reactor's ground wire to detect electric field changes. This electric field probe was only used for PD detection. By setting up the system like this, we can study whether the electric field changes around the post are due to the leakage current from the insulator or from any outside influences. If the electric field signals changes synchronous with the changes of the current in-ground wire means the leakage

Fig. 3.4: Rogowski coil setups.

Table 3.2: Table of test environment information and setup configurations.

Conditions	Segment length	Temperature	Humidity	Wind speed and direction
Field test #1	0.1 ms	-5°C	53%	7km/h North
Field test #2	50 ms	-10°C	62%	2km/h Northwest
Field test #3	50 ms	-5°C	80%	3km/h Northwest

current is strong enough for the discharge phenomenon to occur. Finally, all detected signals are transmitted through coaxial cables to a high-speed ADC unit and all data is stored on a local computer.

Between 2018 and 2019, the time of the three field tests was selected based on different weather conditions. In the first and second field test, the captured signals have been proved to be due to the switching behavior of the DC converters which are not relevant to the partial discharge activities. In the third test, we were able to capture random PD signal from electric field sensors. Table 3.2 shows some environmental information and the oscilloscope configurations for all HVDC substation field test.

(a) Computer Setups.

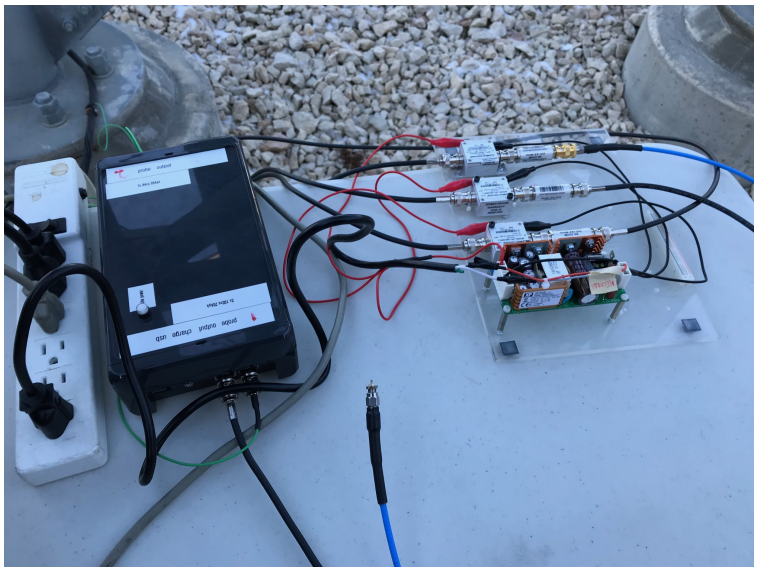

(b) Amplifier and Low Pass Filters Setups .

Fig. 3.5: Data acquisition system setups at HVDC substation.

3.2.1 First Field Test Procedure and Result

At the first visit to HVDC substation in Oct 2018 we implement our monitoring system. The acquisition system was set up on the smoothing reactor of the negative pole of the Bipole II valve

group. On that day, the temperature was about -5°C with 53% humidity, with a speed of 7km/h North wind. And there were no discharge phenomena observed or heard during the test.

Based on the collected data, we noticed that large amplitude and fast oscillation current activities existed along the reactor's ground wire. On the oscilloscope, the maximum current detected was 200 mA. Repeating current signal patterns can be observed in the collected data. The oscilloscope has been set to segment memory mode to record all outstanding signals and the associated time stamps, each segment window is 0.1ms with 20 μS pre-triggered signal and 80 μS post-trigger signal. On the first field test, total number of 250 segmented signal were captured. Some samples of the signal are shown in Figures 3.6 to 3.8.

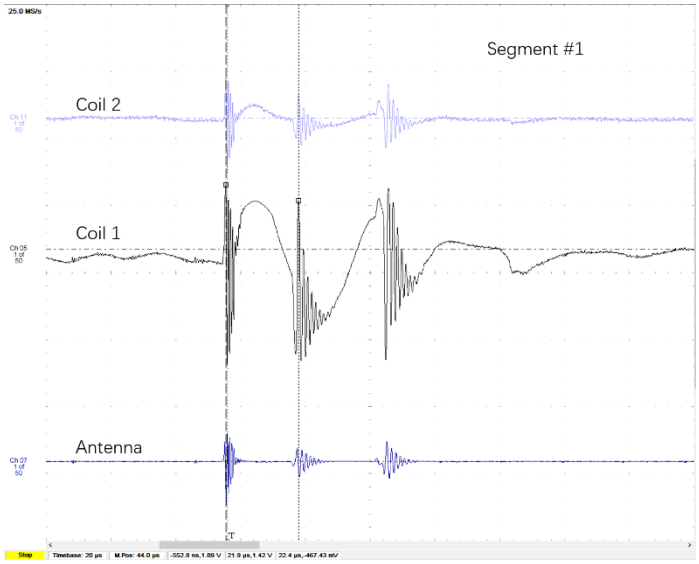

Fig. 3.6: Sample signal #1 from Oct 11, 2018.

From Figures 3.6 to 3.9,we noticed that the recorded signal was formed by some low-frequency signals cascading with some high-frequency signals. In Figure 3.6, the high-frequency oscillation transients exist in all three channels: Rogowski Coil 1, 2, and the electric field probe. The high-frequency oscillation transients from the electric field probe were synchronous with the transient signal from the current in-ground wire, indicating that the leakage current from the insulator post

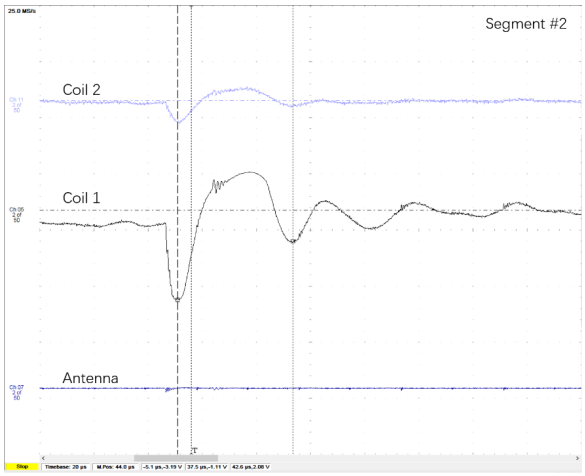

Fig. 3.7: Sample signal #2 from Oct 11, 2018.

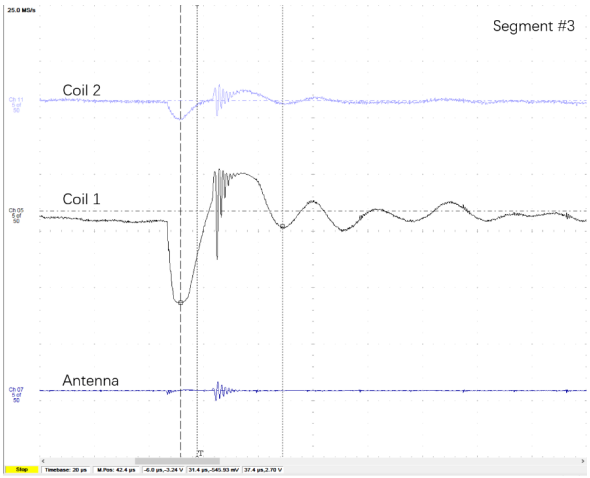

Fig. 3.8: Sample signal #3 from Oct 11, 2018.

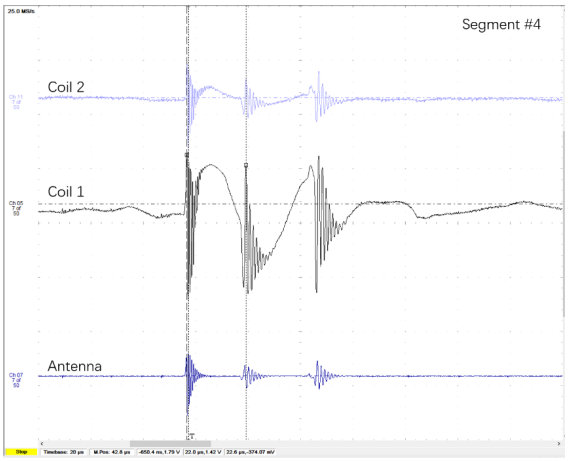

Fig. 3.9: Sample signal #4 from Oct 11, 2018.

generate electromagnetic pluses.

During the filed test at the HVDC substation, about 250 different segmented signals were captured, and some of the collected signal share similar properties (shape, amplitude, and frequency) which means the signal we collected were not purely random. Some common current patterns are shown in Figures 3.6 to 3.8. By study the patterns distributions listed in Table 3.3, it has been appeared that number of signal with 3 transients in one segmented window (3.6) and signal with 2 transients in one segmented window (3.7) are close. This result shows that the signal we collected maybe periodic.

Based on the observation, we applied wavelet decomposition to all 250 signal segments and assorted all captured signals into characteristic groups: signals with one, two, three, four or none fast oscillation transient. The result is shown in Table 3.3. Table 3.3 shows that the total number of signals with two and three fast oscillation transients are very close to each other, and they are the dominant part within the signal which has transients. Therefore, we applied FFT to those segments that have two and three fast oscillation transients to study the characteristic of the transients. The frequency distribution results are shown in Figures 3.10 and 3.11. In Figure 3.10, the FFT results show that the signal with two fast transients has the first transient's frequency mostly located

Table 3.3: Distribution of Signal with Multiple Fast Oscillation Transients.

One Oscillation	Two Oscillation	Three Oscillation	Four Oscillation	None Oscillation
33	53	60	4	100

at 100 kHz, while the second transient's frequency is mostly located at 720 kHz. In Figure 3.11, the FFT results show that the signal with three fast transients has the first transient's frequency located between 1.4 to 1.5 MHz and the second and third transients' frequencies are 720 kHz. This is about half of the first transient's frequency.

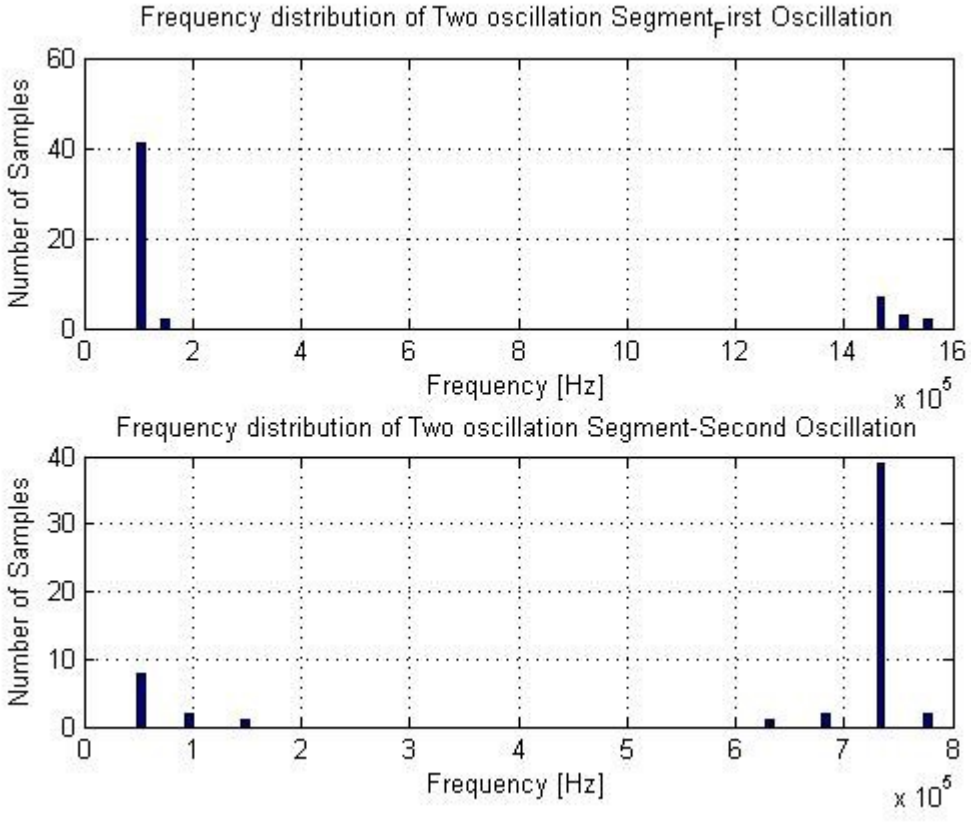

Fig. 3.10: Frequency distribution of two transients signal segments.

Based on the results of FFT, we suspected that these transients might come from a stable and

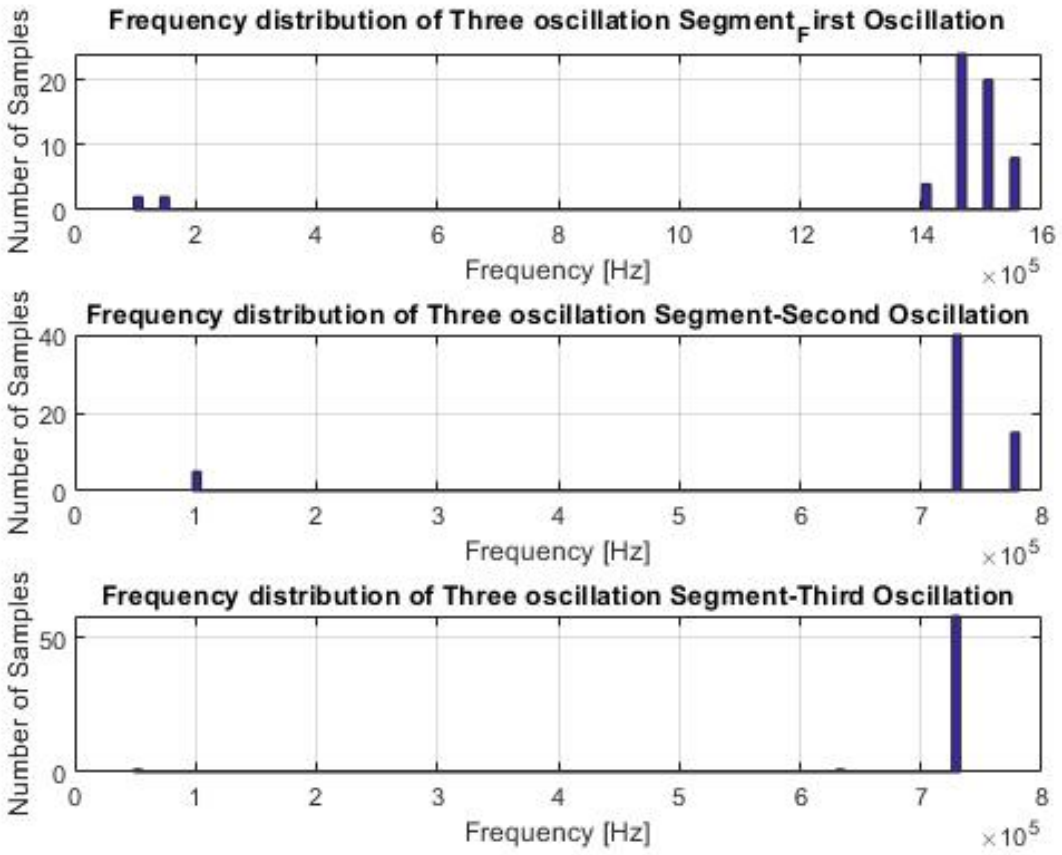

Fig. 3.11: Frequency distribution of three transients signal segments.

periodic source. Thus, we decided to use a larger capture window to see if we could get any periodic pattern in future experiments.

3.2.2 Second Field Test Procedure and Results

In Nov 2018, we completed our second field test at the HVDC substation. The acquisition system was also set up on the smoothing reactor of the negative pole of valve group. The temperature was about -10°C with 63% relative humidity, and the Northwest wind speed was about 2 km/h. During

the test, there were no discharge phenomena observed or heard. In our second field experimental test, we increased our capture period from 0.1 ms to 0.05 s per segment to see if there could be any pattern found in a longer window of time. The results are shown in Figure 3.12. The signal in red is the ground wire current, and the signal in blue shows the electric field. The captured signals show that the transient from the ground wire is a periodic signal and the period of this pattern is about 8ms. Figure 3.13 shows the details of this transient pattern: it starts with a three fast oscillation transient and after about 1.5 ms a two fast oscillation transient appears, then the signal is silent for 6.5 ms. In order to get detailed de-noised signals, the 3^{rd} level of Daubechies 3 (DB3) wavelet decomposition was applied to captured signal to eliminate high frequency noises. The results of wavelet decomposition of signal in Figure 3.12 are shown Figure 3.14 and 3.15. All these transients have almost the same property as the signal in our first measurement test. This proves our first hypothesis that the transient in the ground wire comes from a steady periodic source. In this case, we divided the signal into two parts, three oscillation transient parts and two oscillation transient parts, for further signal processing studies.

3.2.2.1 Signal Part I: Three Oscillation Transient Part

Figure 3.16 shows detailed information about the three oscillations part of the signal. The time difference between these three transients is 23 μs and 27 μs. Clearly, in Figure 3.16 the first transient's amplitude frequency and damping speed are much faster than the other two transients. Using short-time Fourier transformation (STFT) on the signal shown in Figure 3.16, we can get a clearer observation of how the frequency content changes over time. The STFT result is shown in Figure 3.17.

FFT was applied to all captured segments (the same signal processing procedure as in section 3.2.1) and the results are shown in Table 3.4. The first transient's frequency is mostly located between 1.07 MHz to 1.12 MHz, while the second and third transient's frequencies are mostly located at 0.63 MHz and 0.58 MHz - much lower than the first one.

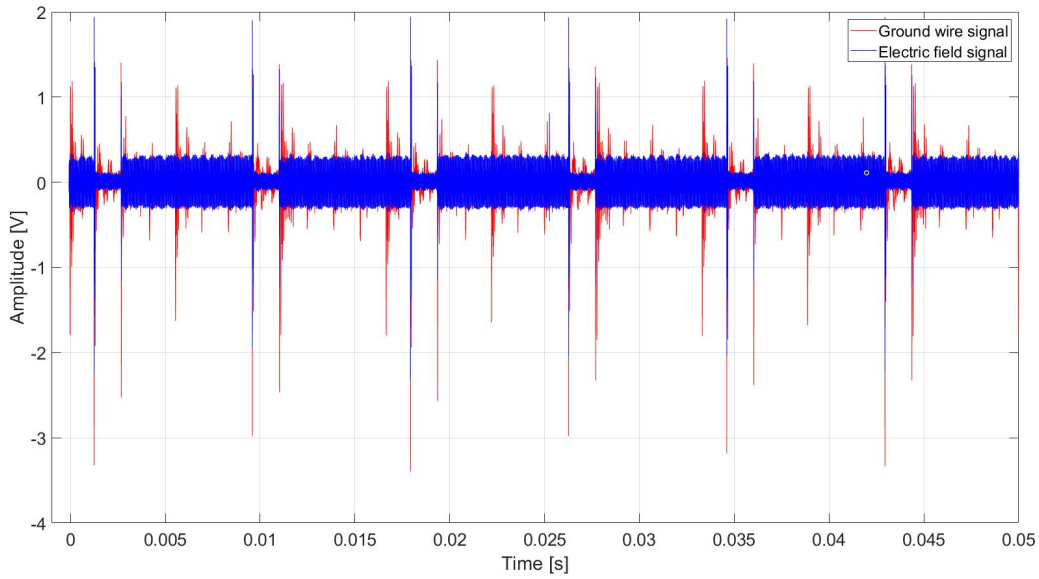

Fig. 3.12: Sample signal captured on Nov 16, 2018.

Table 3.4: Frequency Distribution of Periodic Signal in Fig 3.16.

	Frequency	Number of samples
First transient	1.02 MHz	1
	1.06 MHz	42
	1.12 MHz	17
Second transient	0.63 MHz	60
Third transient	0.58 MHz	60

3.2.2.2 Signal Part II: Two Oscillation Transient Part

Figure 3.18 shows detailed information of the two oscillation parts of the signal. The time difference between these two transients is 11 μs. However, unlike the signal in Figure 3.16, the first oscillation in Figure 3.14 is very small and only lasts for a few micro seconds. The second oscillation looks like a damping sinusoid wave just like the transient in Figure 3.16. By applying FFT to all captured

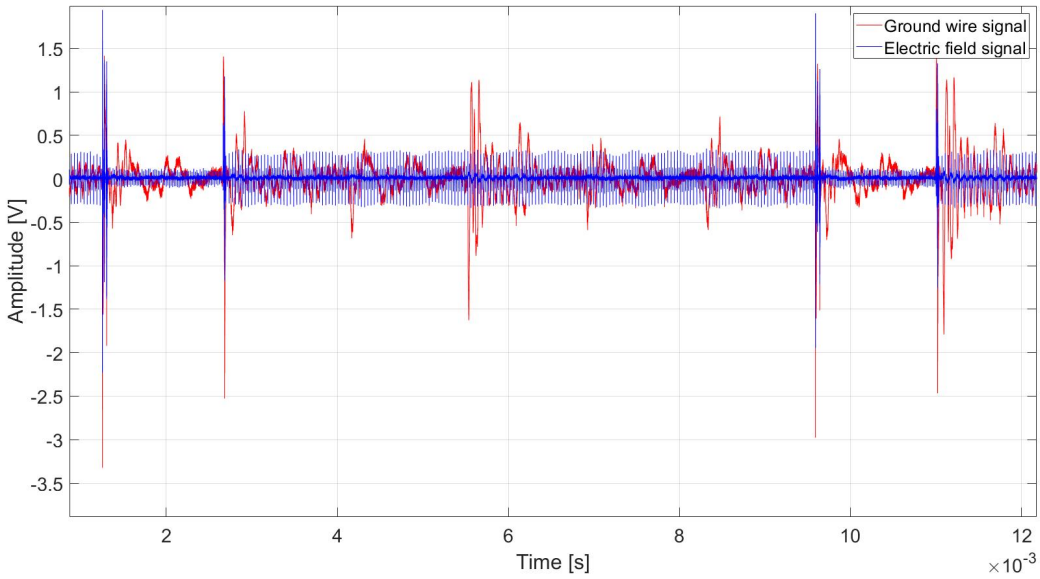

Fig. 3.13: Detail periodic signal pattern from Fig 3.12.

segments the frequency distribution of the second part is 0.63MHz.

3.2.2.3 Correlation with 12 Pulse Converter and Hypothesis

As per the discussion in Sections 3.2.2.1 and 3.2.2.2, the time difference between these signals is about 1.4 ms which is shown in Figure 3.19. Based on the previous measurements we suspect the transients come from a periodic and steady source.

In the HVDC substation a 12 pulse line-commutated converters (LCC) are installed. Figure 3.16 is the equivalent simulation schematic for 12 pulse LCC HVDC converters. Figure 3.19 shows the output voltage from the smoothing reactor. The frequency of the signal in Figure 3.19 can be calculated by

$$f = f_{AC} \times \text{Number of pluses.} \tag{3.1}$$

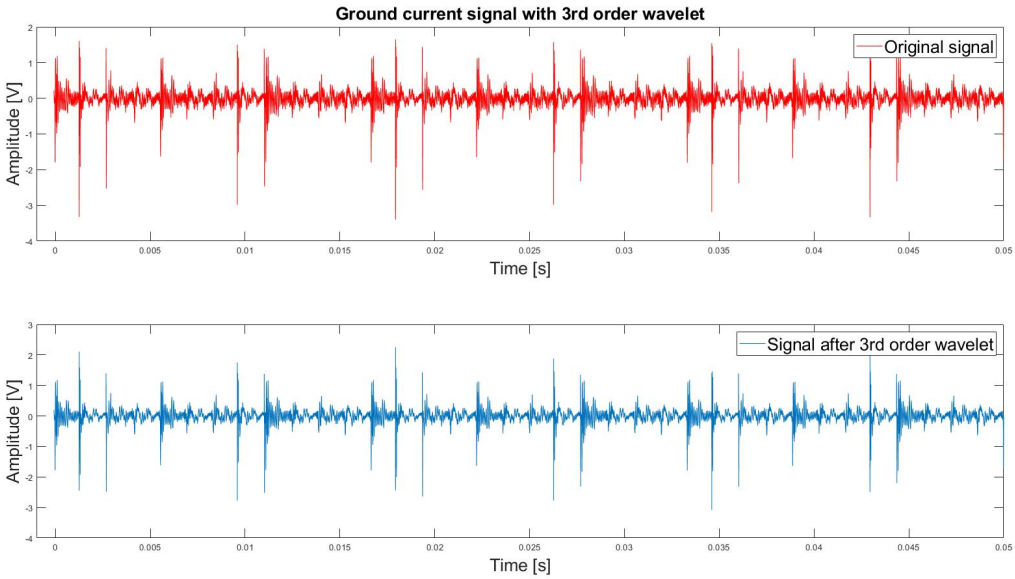

Fig. 3.14: Ground current signal wavelet decomposition result from Fig 3.12.

In this case, $f = 720$ Hz and the period of the signal is 1.38 ms very close to the period shown in Figure 3.19. What's more, the period of the signal shown in Figure 3.13 is about 8 ms that is equal to half of the period of a 60 Hz sine wave which is the output voltage of the converters. Based on the evidence discussed above, our hypothesis is that the transient from the ground wire comes from the influence of the switching behaviour in the converter station.

3.2.3 Third Field Test Procedure and Result

in March 2019, we completed our third field test at the HVDC substation. The acquisition system was also set up on the smoothing reactor of both positive and negative poles of the valve group. The temperature was about -5C with 80% relative humidity, and an East wind with a speed of about 7 km/h. The operation voltage of the positive valve group was 450kV, and the operation voltage of the negative valve group was only 225kV (due to maintenance). During the test, we could hear discharge sounds clearly from the smoothing reactor's posts (both the positive and negative

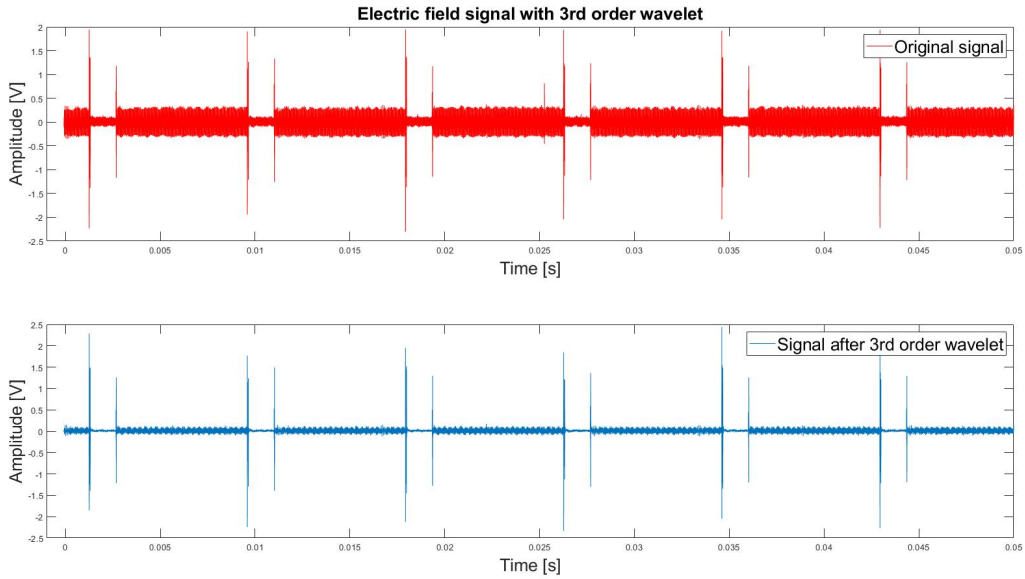

Fig. 3.15: Electric field signal wavelet decomposition result from Fig 3.12.

side) but only from the units is directly connected to the 12 pulse converter valve. However, the discharge was not strong enough to be visibly observed (no visible arcs).

In our third test, we followed the same measuring procedure as the second test. The Rogowski coils picked up almost the same result. However, the antenna probe detected some random monopolar pulses during the test. A sample signal is shown in Figure 3.20. The blue signal indicates the current signal in the ground wire that is captured by the Rogowski Coil, the red one indicates the electric field signal that is captured by the antenna. In Figure 3.20 we also map the signals with a 1.4 ms per division grid to study whether our hypothesis regarding the correlation between transients in the ground wire and 12 pulses LCC converters is true.

From Figure 3.20 we noticed that all the large oscillation transients line up with the 1.4 ms grid, meaning that the time gap between the transients is very close to the period of the signal generated by a 12 pulse LCC converter. This observation proves that there is a good chance the transient from the ground wire is generated by the switching behaviour of the 12 pulse LCC

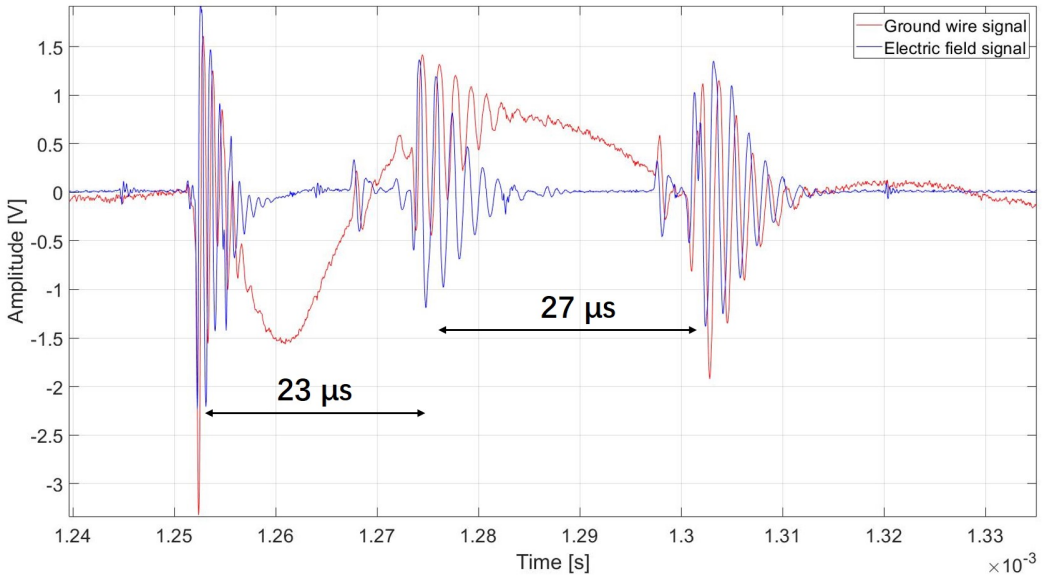

Fig. 3.16: Details of three oscillation transient part of signal in Fig 3.13.

converter. However, in Figure 3.20, there are some monopolar pulses observed at the electric field channel. Both amplitude and apparent timing of these pulses are random. What's more, at the current channel no corresponding signal appears when these random pulses occur. By using the pulse's monopolar characteristic, we successfully separated these pulses from other signals. The distribution of the pulses along the capture window is shown in Figures 3.21 and 3.22.

Figure 3.21 shows the result that we recorded from the negative pole of the HVDC system, and Figure 3.22 is the result from the positive pole. The red line is a 60 Hz Sine wave reference, and the blue line indicates a sample electric field we captured without any random discharge pulse in our third field test. Both Figures 3.21 and 3.22 show that for the oscillation transients we captured from field test 1 and 2, the time between two three oscillation transients is half of a 60Hz sinewave. This proves our hypothesis from section 3.2.2. The black circle in Figures 3.21 and 3.22 indicate the amplitude of the random discharge shown in Figure 3.20. At the negative pole, the amplitude of the electric field pulses are between -10^4 and 10^4 V/m. However, the amplitude distribution

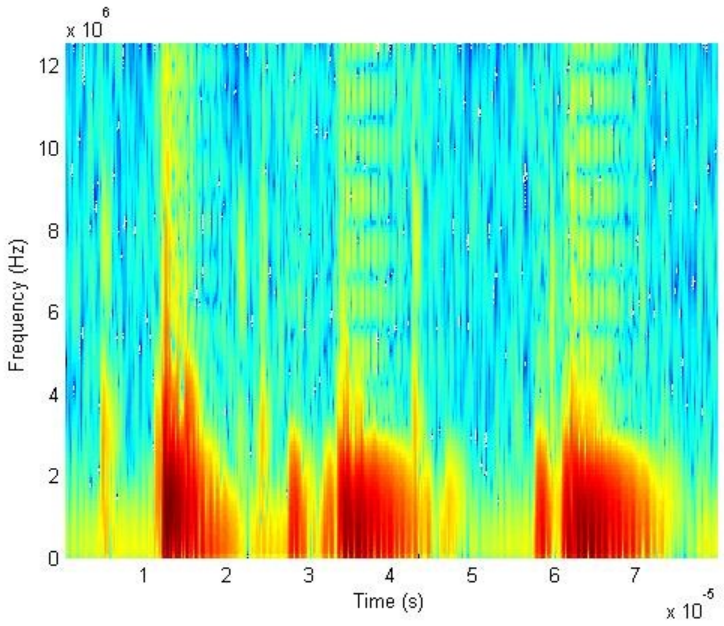

Fig. 3.17: Short Time Fourier Transformation (STFT) of the signal in Fig 3.16.

from the positive pole is much wider; the amplitude is located between -4×10^4 to 1.8×10^4 V/m. We believe the reason the amplitude is lower in the negative pole is that it was only working to half of its captivity.

3.3 Conclusion

After three field tests at the HVDC substation, we found that the discharge phenomena were detectable when specific conditions were met that enabled it to be heard or have arcing visible to the naked eye. We believe the partial discharge that occurred on the insulator stacks is a result of static charge buildup on the insulator sheds (no environmental pollution). When the humidity is high, the static charge buildup on the insulator spreads along the insulator surface and create a conducting path between the smoothing reactor, flange, and ground. Since the flange is a floating metal within this conducting path, the sharp edge of the flange generates corona and causes small

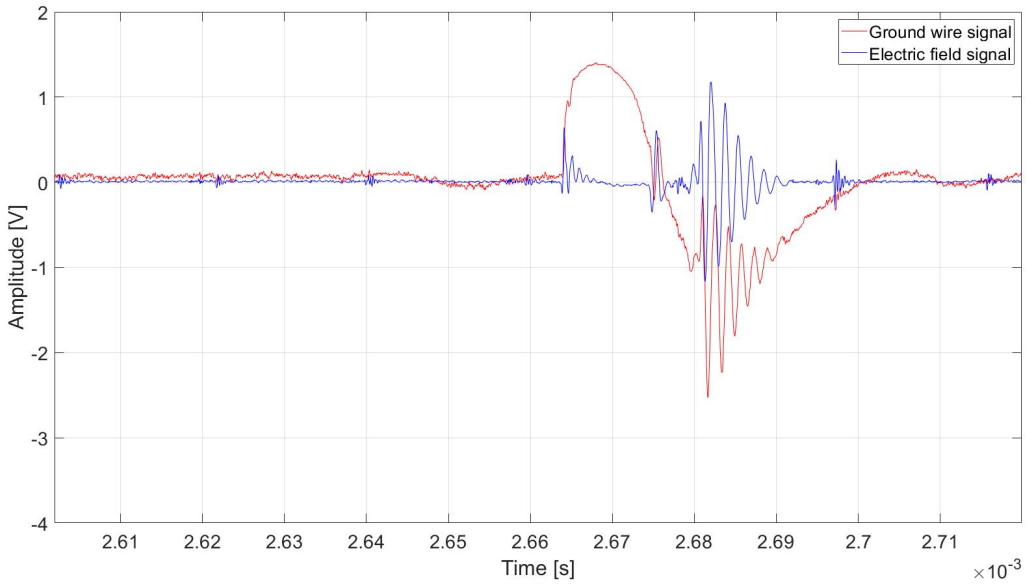

Fig. 3.18: Details of second part of the signal in Fig 3.13.

visible arcs. In the next chapter, a down-scaled lab model to simulate a similar situation to prove our hypothesis is presented and discussed.

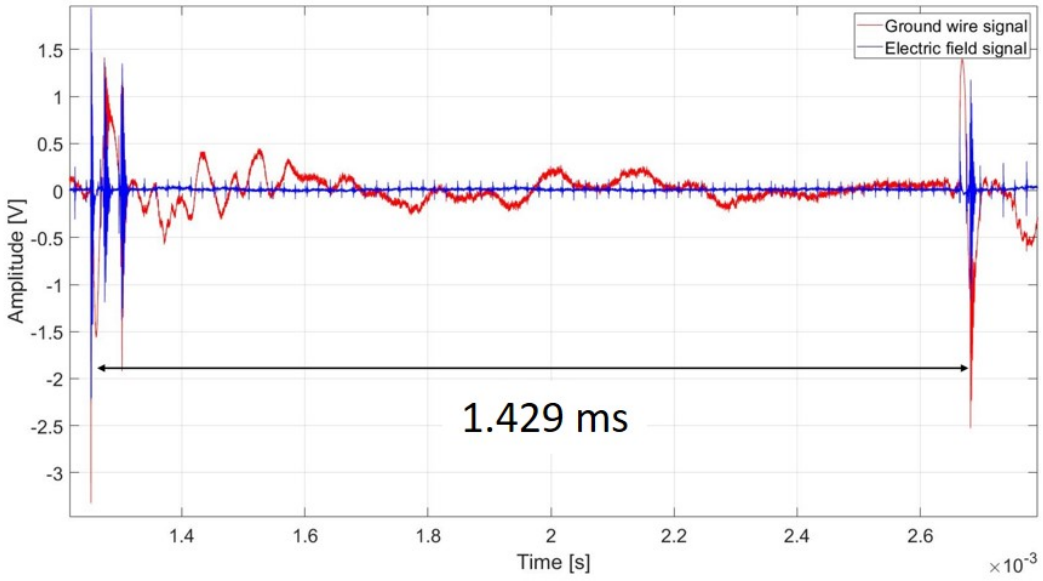

Fig. 3.19: Time gap between oscillation transient in Fig 3.13 .

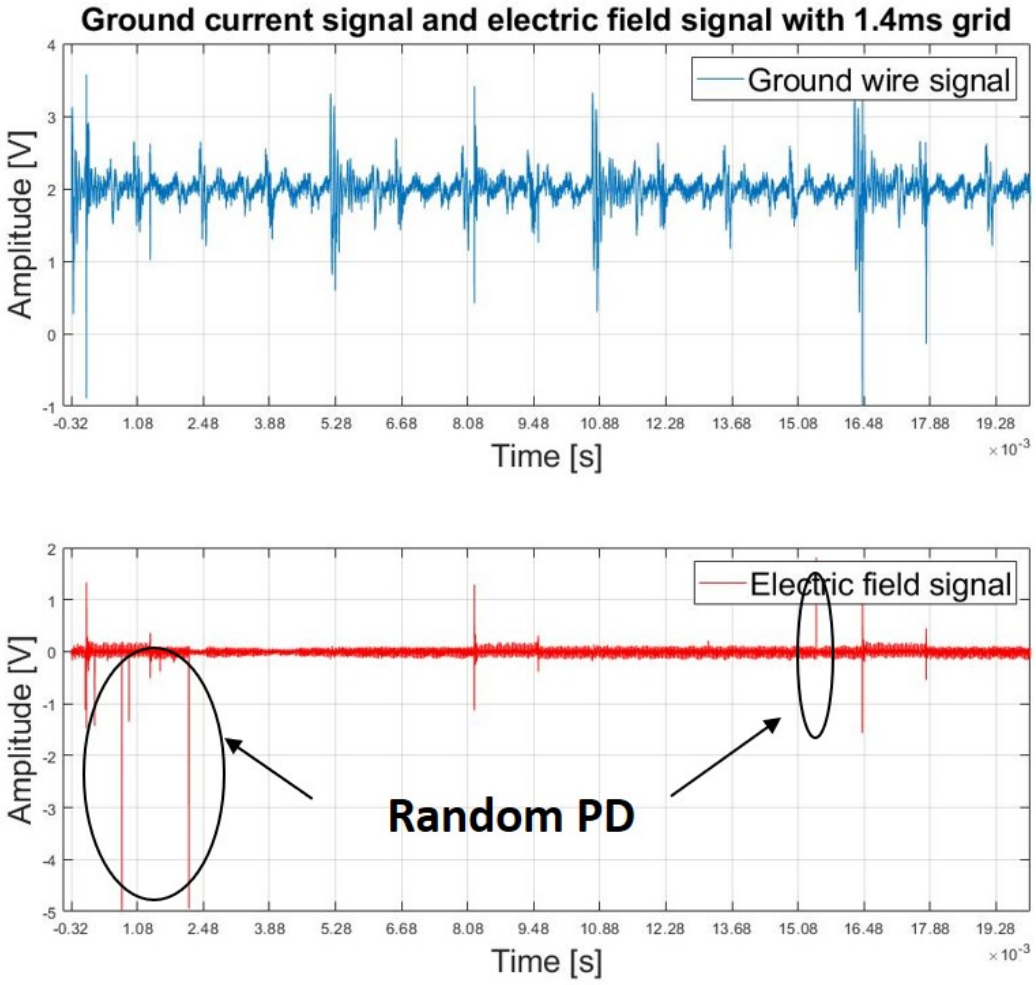

Fig. 3.20: Sample signal from the March 26, 2019 test.

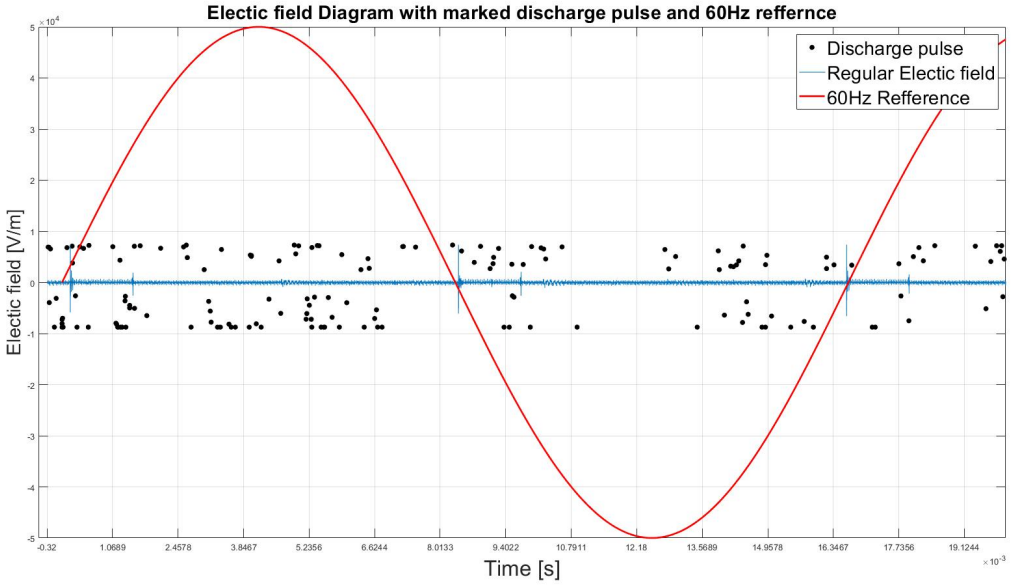

Fig. 3.21: Amplitude distribution of corona recorded on negative pole of HVDC system.

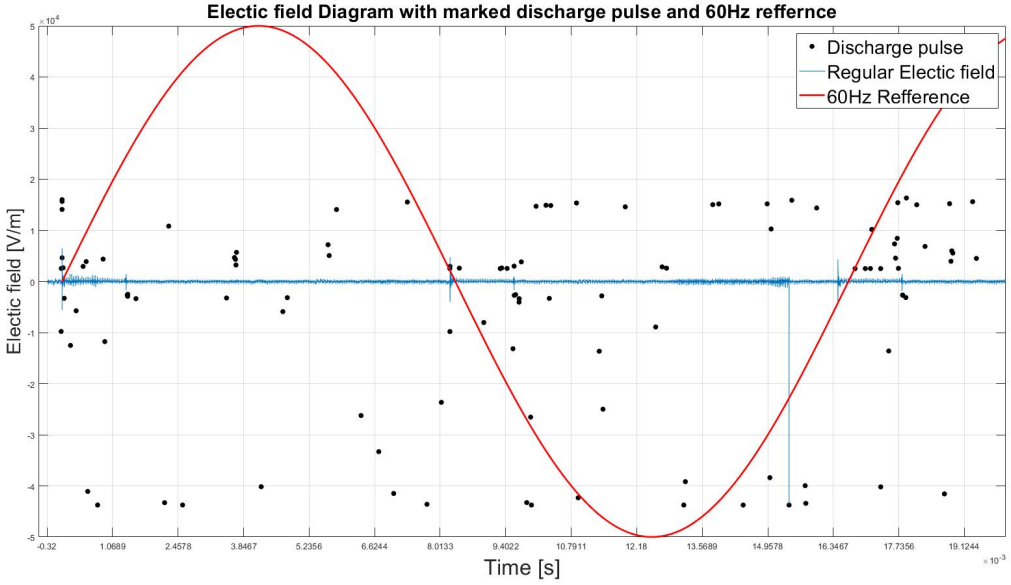

Fig. 3.22: Amplitude distribution of corona recorded on positive pole of HVDC system.

Chapter 4

PD and Flashover Laboratory Experiments

To investigate the hypothesis discussed in Chapter 3, a down scaled insulator testing unit inside a fog chamber was built at the University of Manitoba's McMath High Voltage lab. By adjusting the environmental parameters (temperature and humidity), and injecting free charges to the surface of the insulator, we tired to recreate an environment similar to that at the substation when we observed partial discharge. Ultra-sonic and heated humidifiers were used to adjust the relative humidity levels and the temperature inside the fog chamber. A corona ring of needles was used to apply free charges on the surface of the test sample. The free charges were to simulate and model the charges created by HVDC transmission line that were attracted and trapped on the surface of the insulator. Copper strips and two sharp objects were introduced to create a triple point junction between air, the insulator, and the electrodes which were simulated to model a common corona created by the flange's sharp edge. The details of the experimental setup, methodology, and procedure are demonstrated and discussed in the following sections.

4.1 Experimental Setup

Fiber glass reinforced epoxy resin (FRP), Silicone rubber (SIR) insulator samples were used in the experiments. The samples were all 13 cm long. The details of each sample are shown in Table 4.1 .

Table 4.1: Details of the insulators samples used for PD and flash-over experiments.

Insulator Type	Outer material	Core Material	Total Diameter	Outer Material Thickness
FRP	Fiber glass reinforced epoxy resin	hollow/foam filled	3.2 cm	3.0 mm
SIR	Silicone rubber	Fiber glass reinforced epoxy resin	3.0 cm	3.0 mm

The FRP sample is from a Chance universal hot stick tool. The silicone samples are from silicone covered FRP rods for use as a modular system of suspension type insulators. The relative permittivity of FRP and silicone rubber was assumed as 4.0 and 3.5. Below in Figure 4.1 , a picture of the samples is shown.

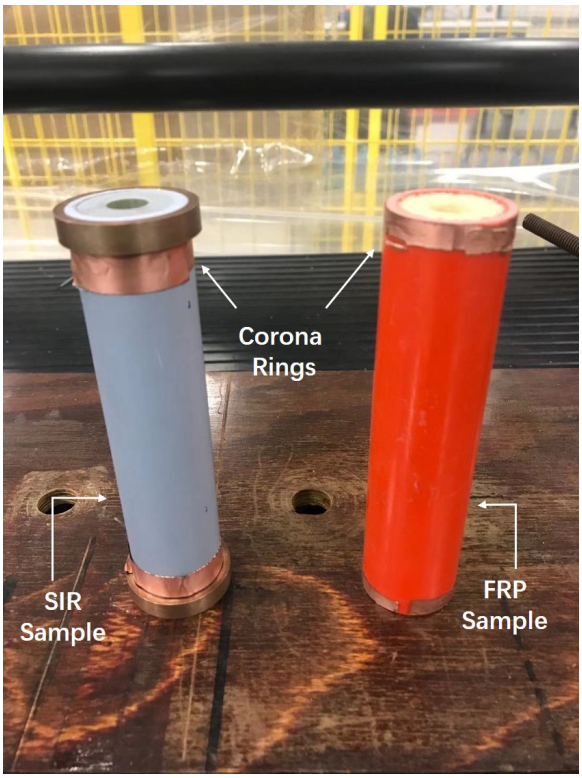

Fig. 4.1: Insulator samples used in PD and flashover experiments.

The effective length of the sample is 11cm, as 1 cm on each side is inserted into the grooves of two metallic, smoothed round electrodes mounted on a wooden setup. Figure 4.2 shows the

experimental equipment used for measuring leakage current and electric field around the test unit.

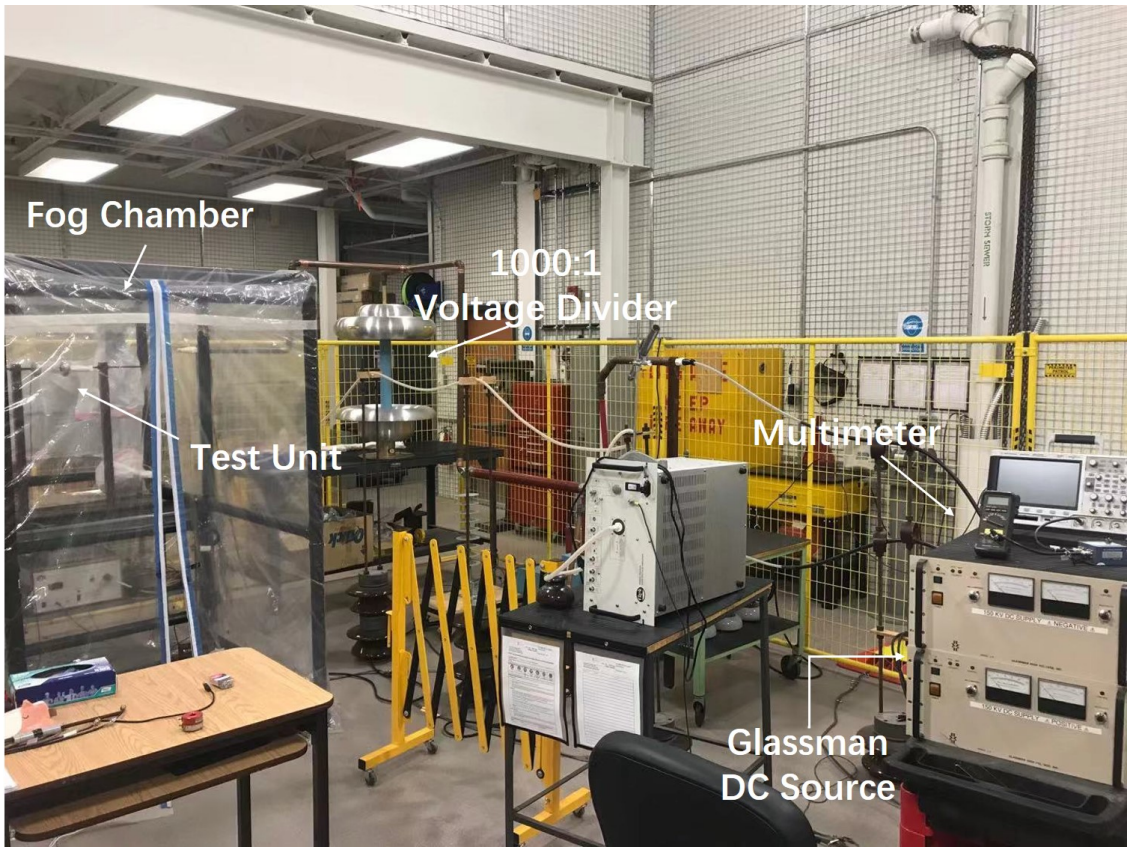

Fig. 4.2: PD and flashover experiments setups.

Figure 4.3 shows the circuit diagram of the laboratory setup used for investigating the partial discharge performance of different insulation samples under different conditions. Two 150kV, 12mA Glassman HVDC sources are used separately to generate positive and negative DC voltages. A 300 kΩ resistor is connected in series with the sample to limit the current of the capacitors during flashover. PDIV voltage is monitored by a multimeter through a mixed resistive-capacitive voltage divider of 1000:1 ratio and 225kV maximum ration with 0.1% DC measurement accuracy. Two current transducers are installed separately on the system's ground wire to monitor leakage current. One is a CT-C1.0-S wideband current transformer, the other is a customized Rogowski Coil. A

TEV sensor from HVPD with 115mV/V sensitivity is installed on the ground to monitor the electric field distributions.

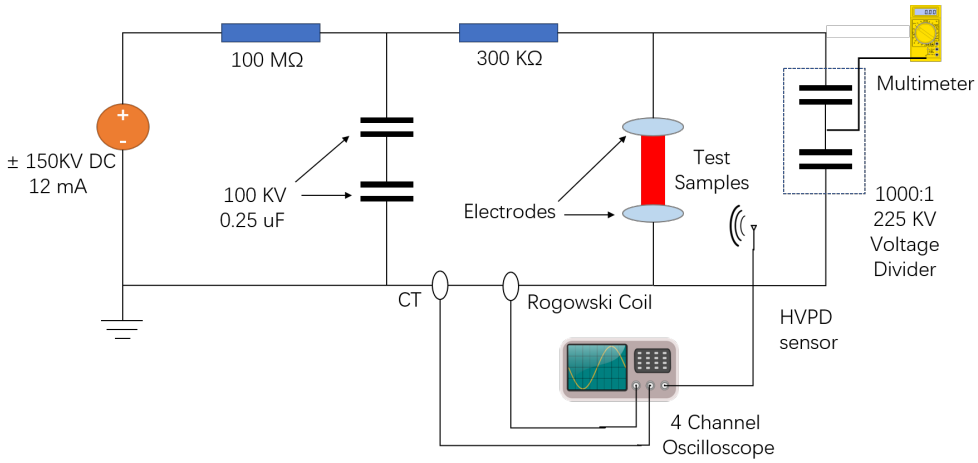

Fig. 4.3: PD and flashover test circuit diagram.

The oscilloscope was programmed in segmented memory mode with a 10G sample per second acquisition rate to record the signals from the CT, Rogowski Coil, and the PD sensor. Each segment is 1μs long, including 400ns pre-triggered and 600ns post-triggered data. The oscilloscope trigger was programmed at the falling edge at -270 mV.

4.1.1 Methodology Testing for Under Humidity Conditions

A fog chamber made by a transparent plastic shield was introduced to simulate the humid environment in the HVDC substation. By changing the humidity inside the fog chamber we were able to study PD and flashover characteristics under different humidity levels. The PDIV and breakdown voltage were expected to have significant variation due to the influence of humidity on charge density and the electric field around the energized electrode. The temperature, humidity, and pressure inside the fog chamber were monitored by a BOSCHE BME280 sensor connected with an Arduino Uno microcontroller. Two humidifiers were controlled by the micro-controller to maintain the hu-

midity level inside the chamber. The fog chamber was activated 20 minutes before the PD and flashover experiments and the humidity level inside the chamber was set to 5% above the desired test value so that the humidifier did not need to operate during the test. After the experiment was complete, the chamber was left open overnight to dissipate the ionized gas inside the chamber. The test was carried out and repeated on 3 different relative humidity levels: dry conditions (20% RH), normal room conditions (50% RH), and humid conditions (¿ 80% RH). Since the temperature inside the lab as different during the tests, the relative humidity levels were converted into absolute humidity and used to keep all test conditions the same.

4.1.2 Methodology Used for Surface Charging

Two different charging methods were investigated to study charge characteristics on the insulator samples. The first method generated space charges in the surrounding air through a non-contact corona discharge source, referred to as a corona ring of needles. It consisted of a 3D-printed polyethylene frame on which 27 connected needles were mounted. The 6.4 cm long needles were distributed around the frame periphery with a 1 cm spacing between every two adjacent needle tips. The needles were symmetrically distributed around the sample surface and the separation distance between the needle tips and the sample's surface was maintained at 5mm during charging. The ring of needles was energized at 20 kV with both polarities of different DC voltages for at least 10 minutes while the two electrodes were kept grounded as per Figure 4.4. The ring of needles was hinged so that it could easily be opened for installation and removal. The ring of needles is displayed in Fig 4.5 in both a closed and open configuration.

The second charging method was to create space charges along the sample surface through direct contact between the sample and the DC voltage source. This method is achieved by energizing one of the electrodes with a DC voltage, while the other electrode is kept grounded. Charging the insulator surface by corona discharge, from nearby energized objects or from direct contact with energized objects, allows for controlling the charge deposition on the insulator surface. Copper

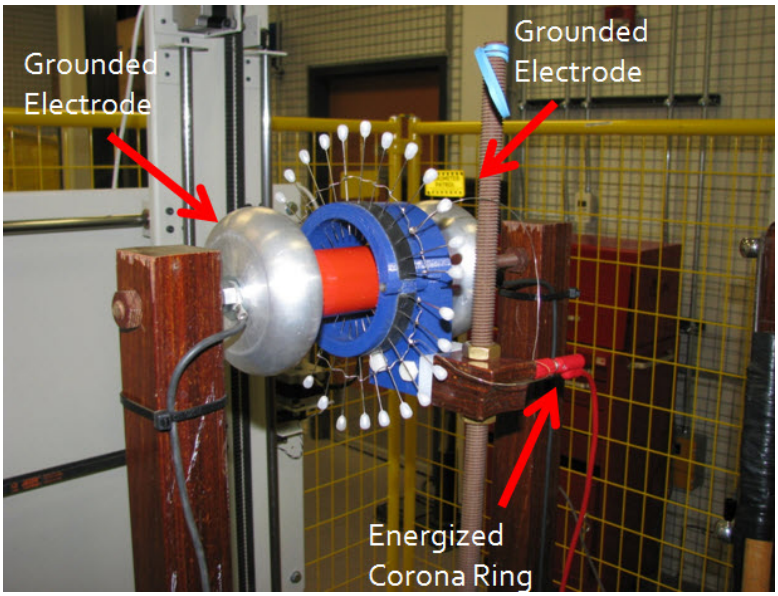

Fig. 4.4: Needles ring to introduce surface charges

strips and two distorted nails were introduced to create a triple-point junction between air, the insulator, and the electrodes. This setup is shown in Figure 4.6 . Tests were carried out without copper strips, with copper strips at both ends, with copper only at the ground or energized side, and with copper strips and nails at both ends.

4.2 Experiment Procedure

4.2.1 PD and flashover test under humid condition

All samples were cleaned prior to testing to ensure that the surface was clean, dry, and neutralized from any charge. The most effective method found to neutralize charge was to take a cloth saturated in distilled water and wrap it around the sample for 2 minutes. The FRP and SIR samples were then rinsed with isopropyl alcohol to clean the surface and ensure no contamination or conductive residue was left.

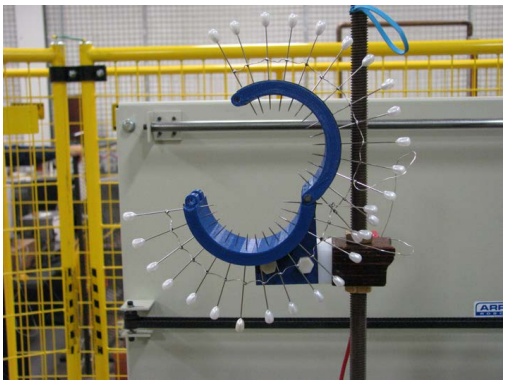

(a) Corona Ring Open.

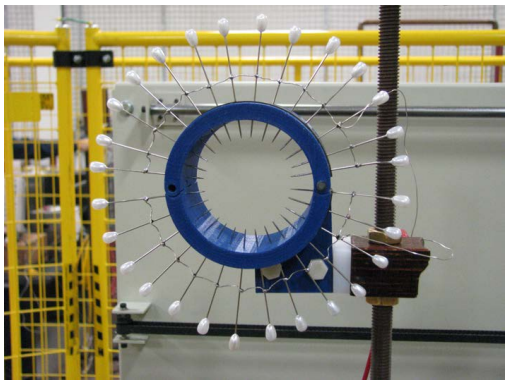

(b) Corona Ring Closed.

Fig. 4.5: Corona ring of needles used for applying non-contact space charge.

The samples to be tested were mounted on the wooden structure, as per Section 4.1. Two identical 0.5cm wide copper strips with bent nails were attached to both ends of the sample. The test structure was sealed inside a transparent fog chamber with two ultra-sonic humidifiers inside, as in Figure 25. The temperature, humidity, and pressure were monitor by a BOSCHE BME280 sensor. The humidity test was carried out and repeated at 3 different relative humidity levels: 20%, 50%, and 80%.

After the relative humidity inside the chamber reached the desired level, the circuit was ungrounded and the voltage was raised at a rate of approximately 500V/s until partial discharge occurred. The PDIV was recorded through a multimeter while leakage current from the sample to the ground and its associated electric field were constantly monitored on an oscilloscope. Next, we continued raising the voltage at the same rate until 15 to 20kV above the PDIV. When the PD appearance frequency was significantly higher than the regular conditions, we began recording the leakage current from the sample to the ground and its associated electric field. The oscilloscope was programmed to use segment memory mode and triggered at negative 270 mV on the falling edge, with a 10G samples per second acquisition rate. Each segment was 1 μs long include with 400ns pre-triggered and 600ns post-triggered data. Typicaly, we recorded 128 to 256 segments before we

Fig. 4.6: SIR Sample with Pre-stressing setup

moved to the flashover test.

After the PD test, we kept raising the voltage at the same rate until the flashover occurred. The flashover leakage current was recorded on the same oscilloscope, triggered at negative 500mV on the falling edge with segment windows of 100 μs (40 μs pre-triggered and 60us post-triggered data). The tests terminated after 10 flashover occurred. Samples were replaced if there was any significant damage on the surface. Degradation of the FPR samples was experienced after 4 to 5 tests (40 – 50 flashovers).

4.2.2 PD and Flashover Test with Surface Charge

All samples were free of surface charges before running the experiments. This was achieved by removing any deposited residual charges by wrapping the sample with a wetted (distilled water) piece of cloth for 2 min, then cleaning the surface with isopropyl alcohol. Extra care was given

not to rub the surface as the friction from wiping can cause significant surface charge. Instead, the surface was rinsed and dabbed lightly. The ring of needles was mounted symmetrically around the sample at the desired location, then the needles were energized with a 20kV DC voltage of both polarities. The duration of the applied voltage to the needles was 10 min. Afterwards, the voltage source was turned off, grounded, and the ring of needles was carefully removed - without touching the insulator. After inducing space charges using the ring of needles, the flashover circuit was ungrounded and the voltage was raised at a rate of approximately 500V/s until partial discharge occurred. The PDIV, PD signal recording procedure followed exactly the same steps as per Section 4.2.1.

4.3 Conclusion

This chapter introduced the PD and flashover laboratory experiments setups and the methodology of test when introduced humidity or free surface charge. By following the described experiments procedures, we preformed PD and flashover test with humidity or free surface charge influences successfully. From the test result, we were able to identify the relationship between partial discharge and humidity and free surface charge influences. Detailed results and conclusions are demonstrated and discussed in the next chapter.

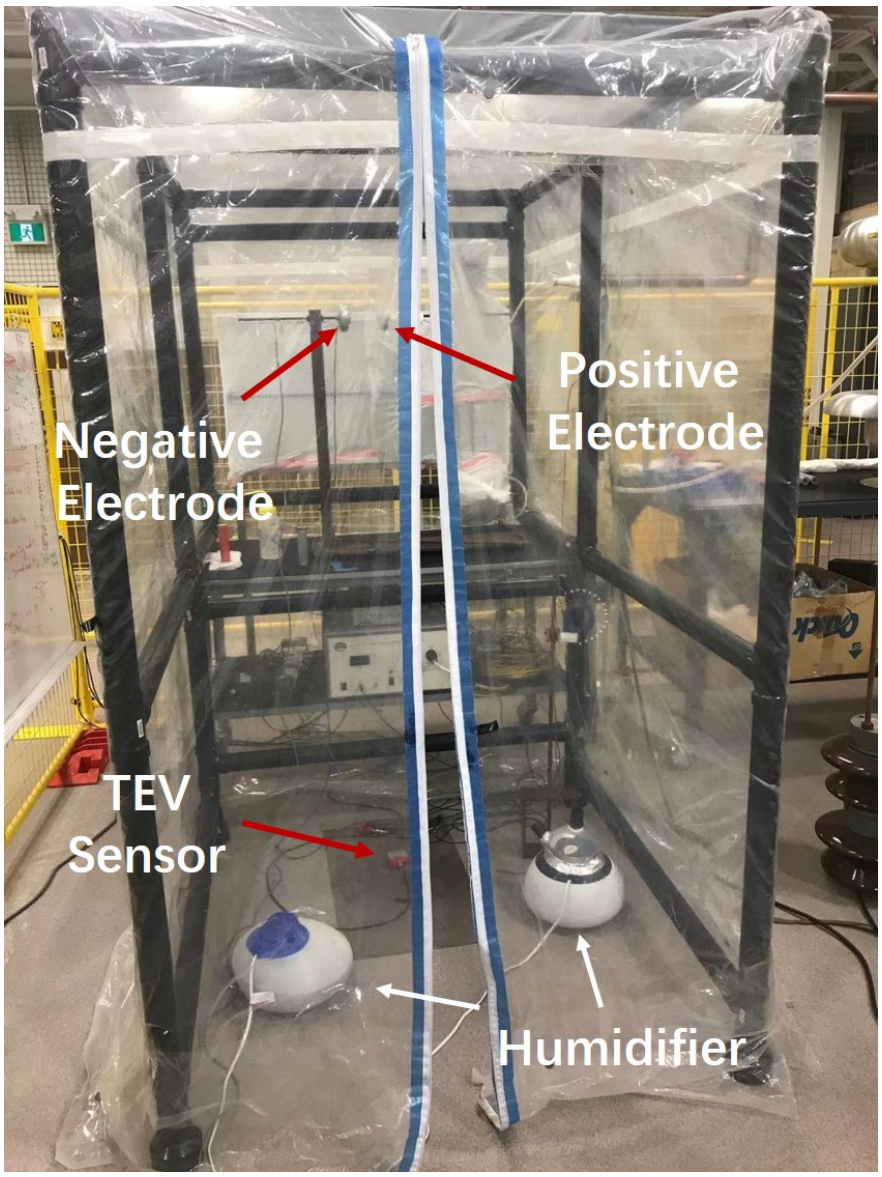

Fig. 4.7: PD and flashover test fog chamber.

Chapter 5

Results and Discussion

In the previous chapter, an experimental test plan for finding the relationship between PD and environmental influences was presented. The experiment with fog chamber setup was designed to model corona under humid environments, including two different test units, an air insulted system as the control group, and the FRP test unit as the desired test group. The experiment with corona ring of needles setup was designed to model corona under surface charge influence that was only tested with the FRP unit.

The results show that the proposed test plan is well able to describe the relationship between PD activities and environmental influences. Detailed results and conclusions are demonstrated and discussed in the following sections.

5.1 HVDC PD Test Under Humid Environment

The results of PD and flashover tests on the insulator samples under different humidity levels are presented and discussed in this section. To present the results, TF mapping, time, discharge magnitude model, and box plot figures are used. TF mapping figures show each individual PD pulse's location on an equivalent time and frequency mapping system. Time and discharge magnitude models show the time of the previous discharge as a function of the discharge magnitude. The box plot figures show the range of PDIV and flashover voltage which include the maximum, minimum,

and median of the data.

5.1.1 Results of Air Insulated Test Unit (Control Group)

An air insulated test setup was used as our control group to prove the environmental influences on different insulation materials. Figure 5.1 shows the setup configurations, the attached corona ring and needles were used in all our lab experiments as a artificial PD source. Table 5.1 shows the PDIV and flashover voltage of the air-insulated test unit with a pre-stressing setup under different humidity levels (25%RH, 60%RH, and 80%RH). The room temperature was 22°C. Since the experiment setup was symmetric, the source was only energized with negative voltage.

Fig. 5.1: Air insulated test unit

Table 5.1: PDIV and Flashover Voltage of Air Insulated Test.

Conditions (T = 22°C)	PDIV	Flashover voltage	Leakage current at PDIV
20% RH	-52 kV	-72 kV	0.2 mA
60% RH	-52 kV	-72 kV	0.2 mA
80% RH	-53 kV	No Flashover up to -90 kV	0.5 mA

Figure 5.2 shows box plots for the PDIV and flashover voltage of Table 5.1. While the environmental humidity increased, the negative PDIV slightly decreased, although not significantly. However, the flashover voltage decreased significantly when the humidity increased. When we increased the humidity inside the fog chamber to 80%RH, at -90 kV, PD activity is strong and frequent, but flashover cannot be observed.

Figure 5.3 shows the results of the TF mapping of the PD signal of the air-insulated test unit. From the plot, we noticed that the PD signal under three different humidity levels were mixed together in the TF mapping system, making it impossible to use K-means clustering technique to separate them from each other. Figure 5.4a is the discharge magnitude as a function of the time to the previous discharge. This plot helps us understand the relationship between the partial discharge's magnitude and appearance frequency. In Figure 5.4b, we noticed that when RH is higher, the time to the previous PD is much smaller than when the RH is low. When RH is 80%, most of the PD signal's Δt lays between 0 to 0.05s. When RH is 60%, most of the PD signal's Δt lays between 0 to 0.3s.And, when RH is 20%, PD signal's Δt speared between 0 to 6s.

5.1.1.1 TFQ 3D Map Analysis

Figure 5.5a is the Time-frequency-charge (TFQ) 3D map results. Despite that the tests were performed under three different humidity levels (RH = 20%, 60%, and 80%), the projected data points from all three tests were grouped together. Figure 5.5b is the YZ plane of the 3D map system shown in Figure 5.5a. This figure shows a function of the relationship between signal total charge magnitude Q and equivalent frequency F. All three test results follow a curve with exponential

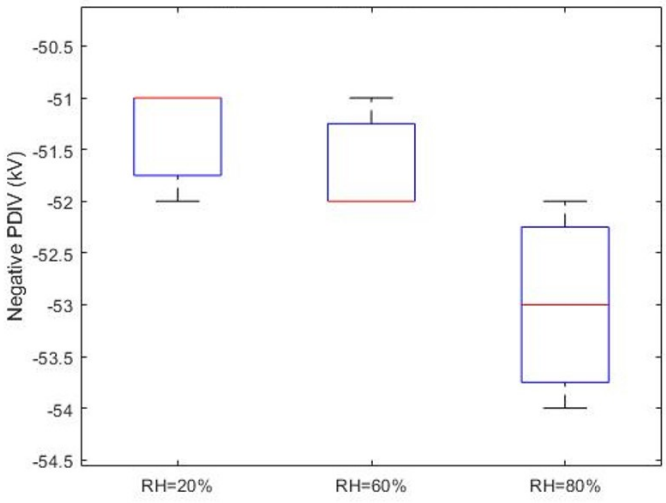

(a) Negative PDIV Under Different RH.

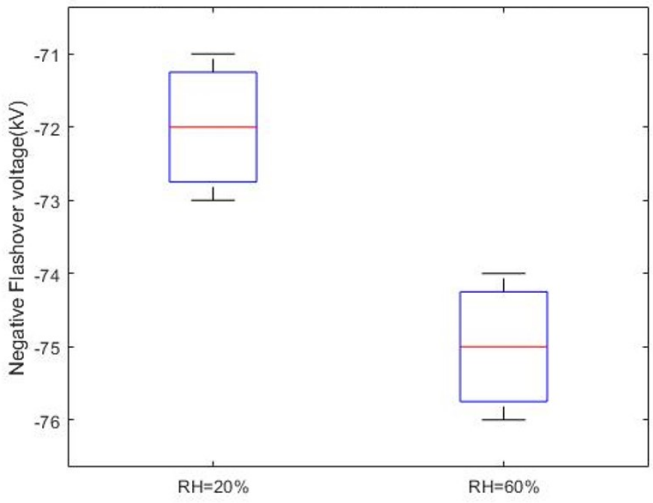

(b) Negative Flashover Voltage Under Different RH.

Fig. 5.2: Boxplot of PDIV and flash over voltage of air insulated test unit under different RH.

decay as the pulse's equivalent frequency increases. The difference in the decay curve among the three tests is negligible.

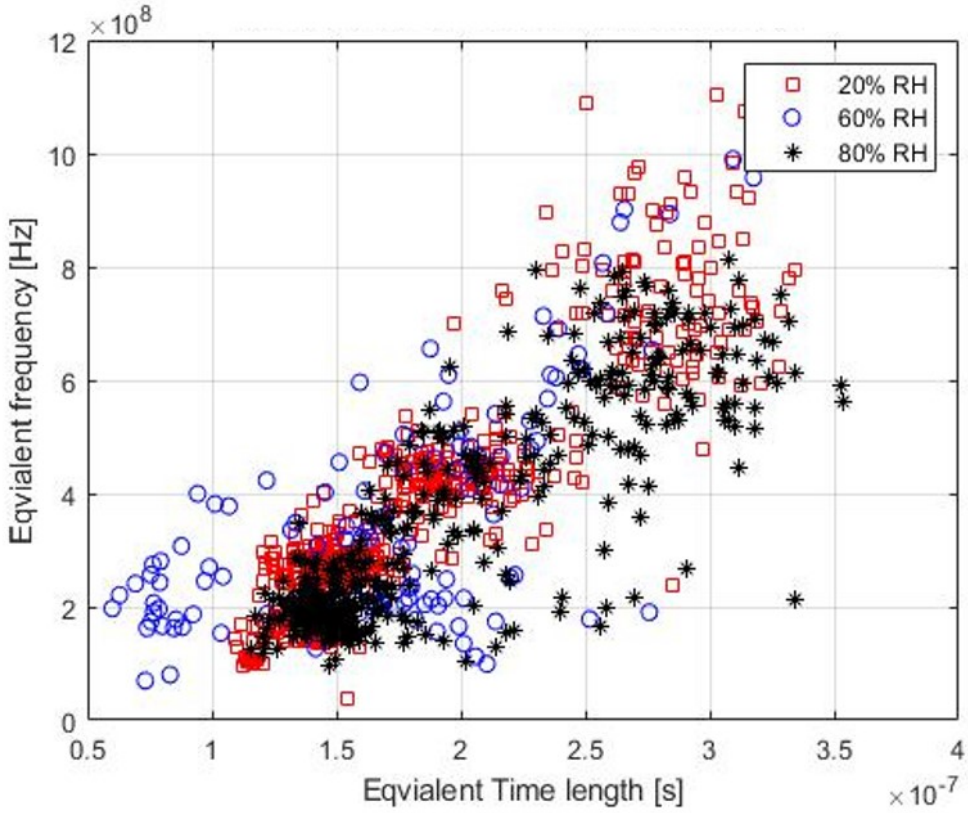

Fig. 5.3: TF map of PD Signal of air insulated test unit under different RH

5.1.2 Result of FRP Test Unit

5.1.2.1 PDIV and Flashover Voltage

Table 5.2 shows the PDIV and flash over voltage of the FRP test unit with pre-stressing the set-up (as per Section 4.1) under different humidity levels. The experiment setup was symmetric and the source was only energized with negative voltage. Since the room temperature varied during the tests, the chamber's relative humidity setting was based on the absolute humidity conversion of the setting in Section 5.1.1.

From Table 5.2 we noticed that as the RH in the fog chamber increased, both the PDIV and

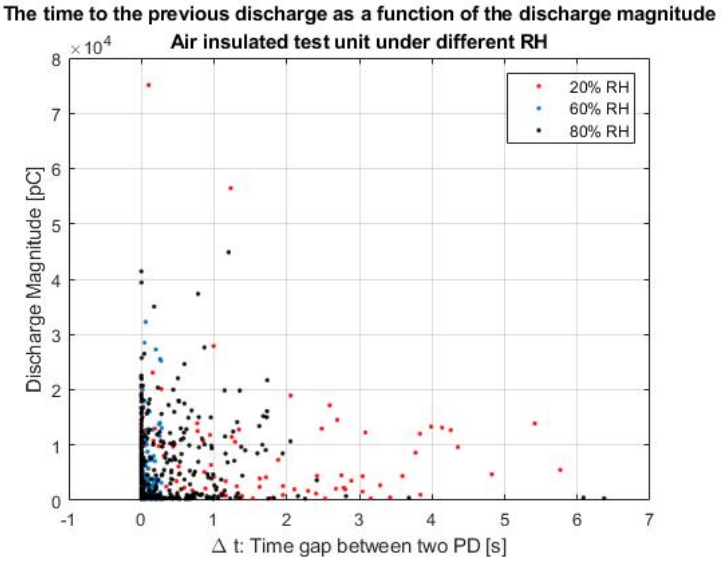

(a) Original plot.

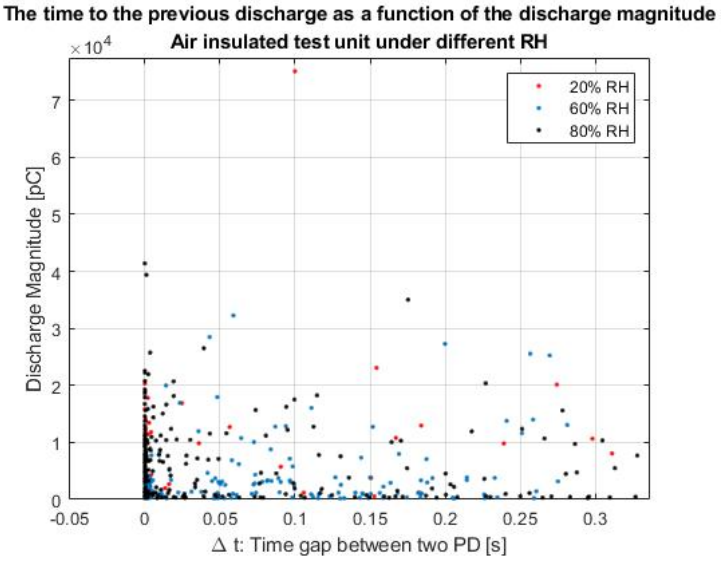

(b) Zoomed version of Fig 5.4a Δt with rang 0 to 0.4S.

Fig. 5.4: Relationship of PD time gap and charge magnitude - air insulated test unit under different RH.

flashover voltage dropped significantly. The result of PDIV was the same as the test in Section 5.1.1; when we increased the humidity inside the chamber, the PD activities became stronger and

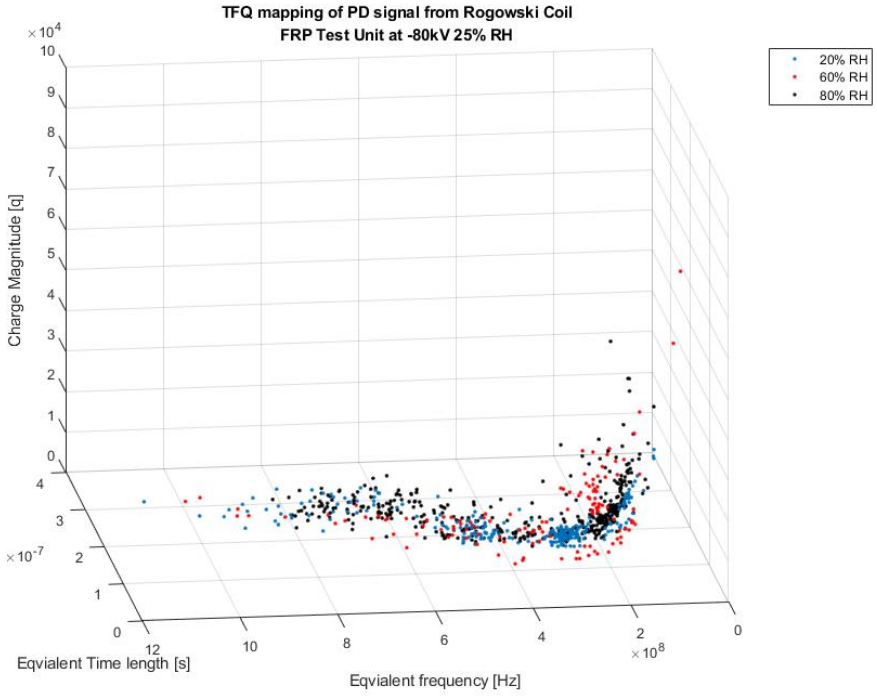

(a) 3D map.

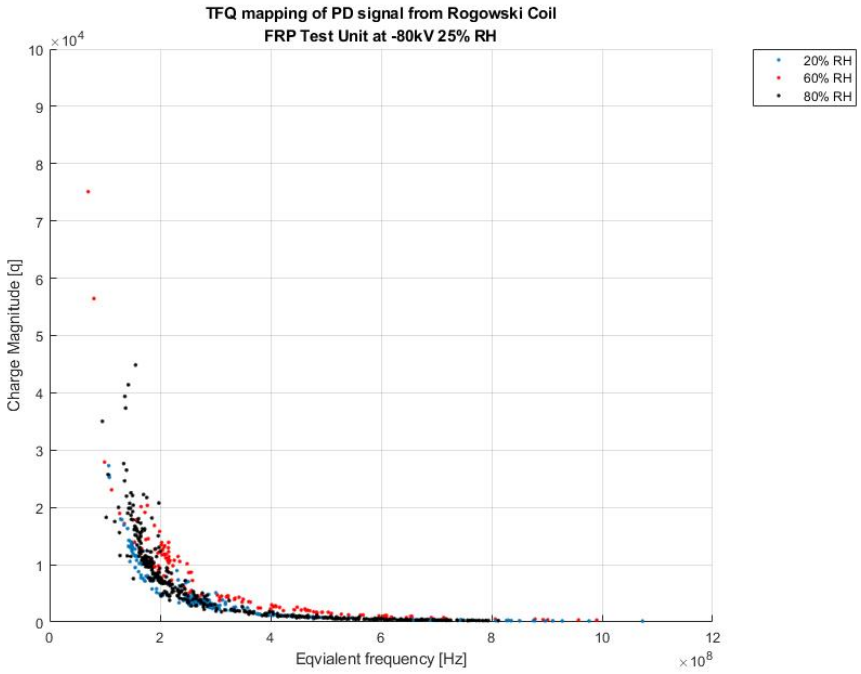

(b) Function of signal total charge magnitude Q and equivalent frequency F

Fig. 5.5: TFQ 3D map of PD signal of air insulated test unit under different RH.

Table 5.2: PDIV and Flash Over Voltage of FRP Unit Under Different RH.

Conditions	Absolute Humidity	PDIV	Flashover voltage	Leakage current at PDIV
20% RH 19°C	4 g/m^3	-60 kV	-83.5 kV	0.5 mA
60% RH 20°C	12 g/m^3	-55 kV	-80 kV	0.2 mA
80% RH 19°C	16 g/m^3	-45 kV	-73 kV	0.2 mA

more frequent. When we increased the humidity inside the fog chamber to 90% RH, at -60kV, audible cracking noise was heard during the test. The sound didn't stop until the system reached flashover, and it appeared again when he system recharged to -40 kV after flashover.

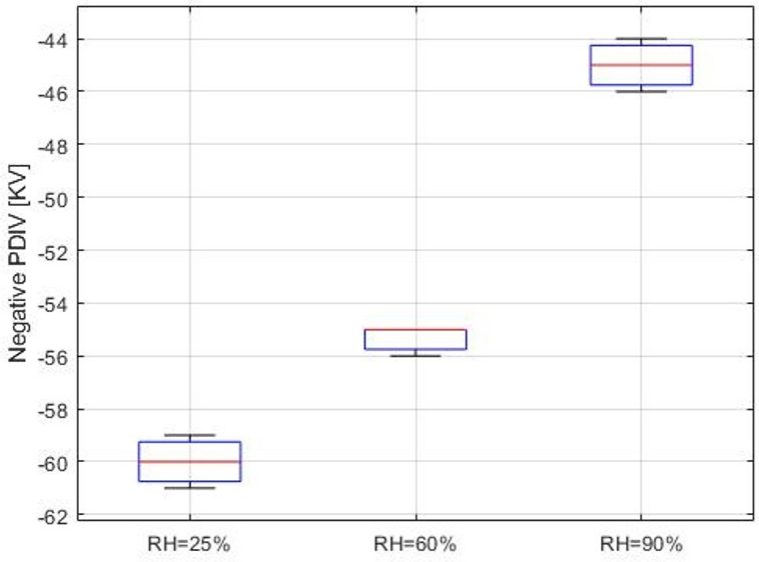

(a) Negative PDIV under different RH.

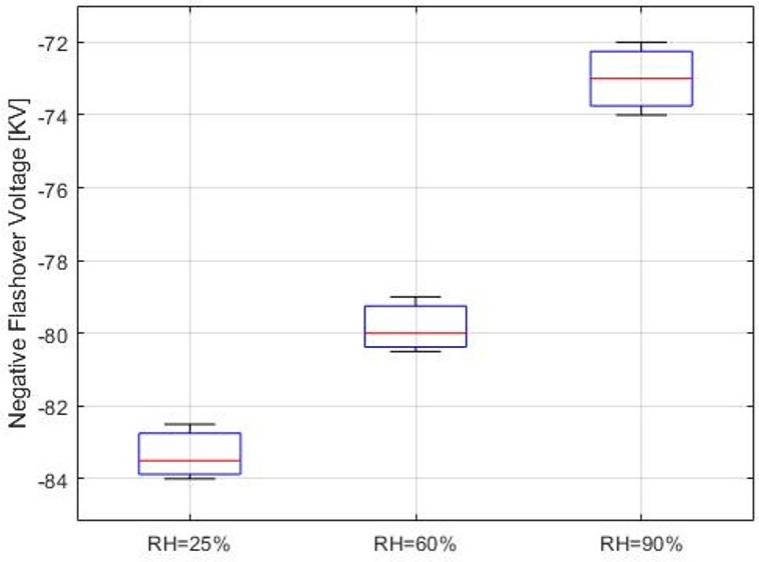

(b) Negative flashover voltage Under different RH.

Fig. 5.6: Boxplot of PDIV and flash over voltage of FRP test unit under different RH.

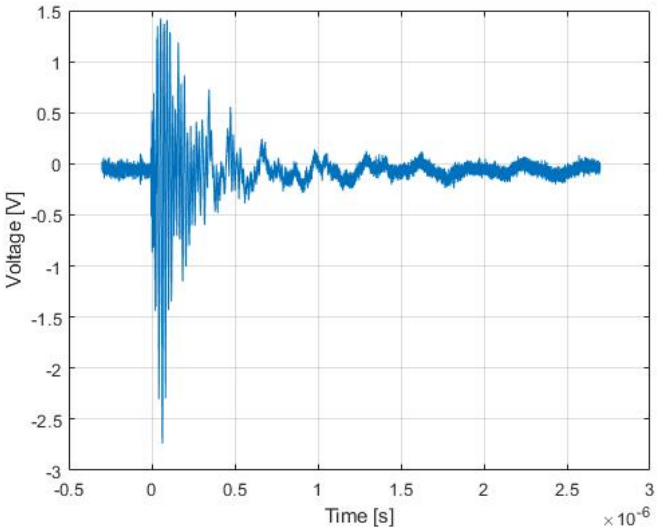

(a) Current with high frequency and short duration.

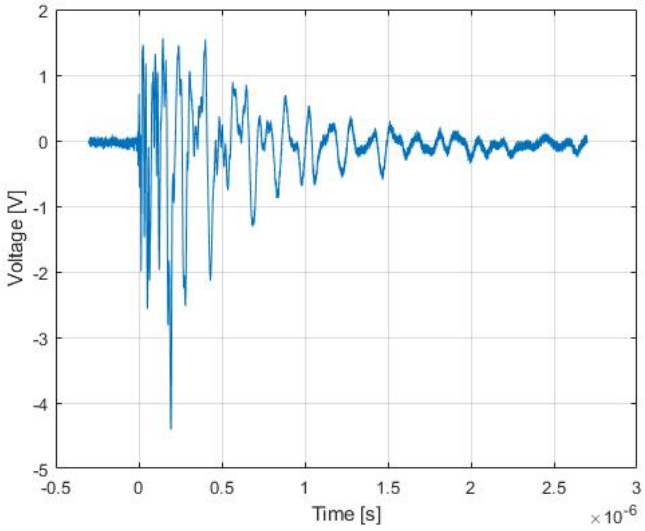

(b) Current with low frequency and long duration.

Fig. 5.7: Two different shape of current from FRP sample PD tests at low RH Levels.

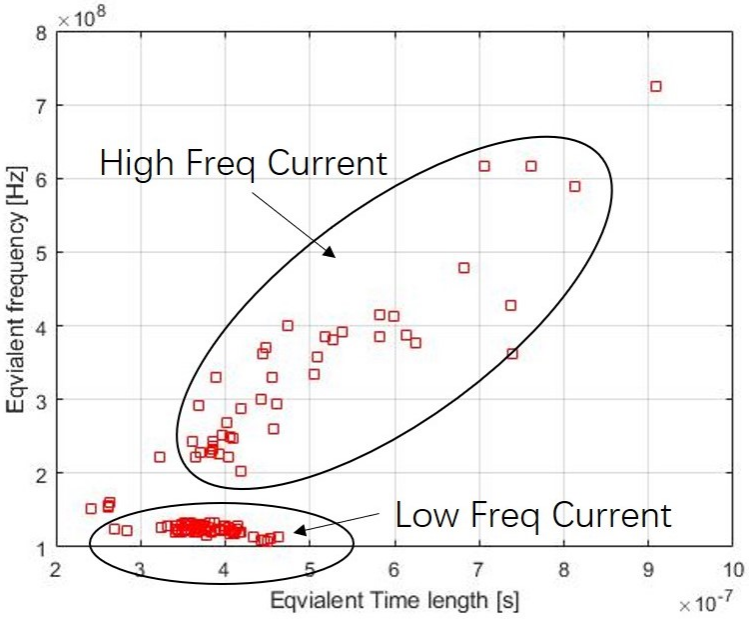

Fig. 5.8: TF Map of PD signal of FRP test unit at -80kV 25% RH.

5.1.2.2 TF Map and PD Frequency Study

In low RH test environment (20% RH in 19°C degree), we noticed that the leakage current had two different shapes. One is a high frequency with short duration, and the other is a low frequency with long duration, shown in Figure 5.7. These two types of discharge current were significantly separated from each other in the TF map system, as per Figure 5.8. In high RH test environments (above 60% RH), we noticed that the leakage currents had similar shape: a small and low-frequency pulse, as per Figure 5.11a. Sometimes there were multiple pulses contained within one current segment, as per Figure 5.11b. Figure 5.9 shows the results of the TF mapping of the tPD signal of the FRP unit under different RH conditions. From the plot, we noticed that the TF plot of 25% RH PD signals was quite far apart from the plot of 60% and 90%. The TF plot of 60% and 90% RH PD pulses were grouped together in the system. The TF map results prove that under high humidity environmental conditions, the characteristics of PD pulses can be changed even with changing the

source of PD.

Figure 5.10 shows the discharge magnitude as a function of the time of the previous discharge. The blue dots indicate the discharge magnitude and its associated Δt (time gap between two PD pulses) in dry environmental conditions (RH = 25%). The black and red dots indicate the discharge magnitude and its associated Δt under humid environment conditions (RH > 50%). With Figure 5.10, we noticed that the results of this test are similar to previous control group tests described in section 5.1.1. When the RH level was high, the time gap between the two PD pulses was significantly smaller than the results from the test conducted under dry environmental conditions. What's more, the results in the figure also show that the magnitude of the PD pulse is larger when the PD happens under low humidity.

Based on the results of Figure 5.10, we performed another test on FRP insulators to study the humidity influence on PD activities. We fixed the source voltage at -70 kV and changed the humidity levels inside the fog chamber. An oscilloscope was used to record the time tag and magnitude of the pulses when PD occurred. The experiment has 4 stages:

- The relative humidity levels inside the fog chamber was leveled up to 90% before the experiment and started monitoring PD activities from oscilloscope. The results are shown in Figure 5.12.

    1. Turned off the humidifiers, opened the chamber and let RH level dropped to 70% RH.
    2. Turned on the humidifiers, closed the chamber and leveled RH level to 80% RH.
    3. Turned off the humidifiers, opened the chamber and let RH level dropped to 60% RH.
    4. Turned on the humidifiers, closed the chamber and leveled RH level to 80% RH.

From Figure 5.12, we noticed that the PD activities were detected and been found with high repetition rate only in the environment with 80%RH and above at -70kV. When the chamber was opened and the RH level below 70%, PD activities were not very active.

5.1.2.3 TFQ 3D Map Analysis

Figure 5.13a is the TFQ 3D map result, and Figure 5.13b is the YZ plane of the 3D map system of Figure 5.13a. Figure 5.13b shows the relationship between signal's total charge magnitude Q and its equivalent frequency F. The location of the projected data points from high humidity ($RH > 50\%$) tests on the 3D space is quite different from the test results under dry environment ($RH < 30\%$) conditions. Overall, PD pulses from tests under high-level humidity environments have lower charge magnitude, but the equivalent time T and equivalent frequency F are much higher than the tests under dry environments. All three test results follow a curve with exponential decay as the pulse's equivalent frequency increase as per Figure 5.13b. The decay speed of test under dry environments is faster than the test under high humidity level environment. The decay curve of test under 60% RH and 90% RH were almost identical.

5.1.3 Cross Analysis Between Control And Test Group

From Tables 5.1 and 5.2, we noticed that the humidity level did not affect the PDIV of the control group (air-insulated) much, but it had a significant effect on the PDIV when we put an FRP insulator between the two electrodes. When we increased the humidity level inside the fog chamber, the flashover voltage of the control group (air-insulated) increased as well, and at 90% RH, we even could not reach the flashover point by using the existing experimental setup. On the other hand, the result of the flashover test of the FRP test unit was quite the opposite: as the humidity level increased, the flashover voltage dropped significantly. From Figure 5.4 and 5.10, we noticed that on both tests, as the humidity level increased, the PD activities became more frequent and easier to observe.

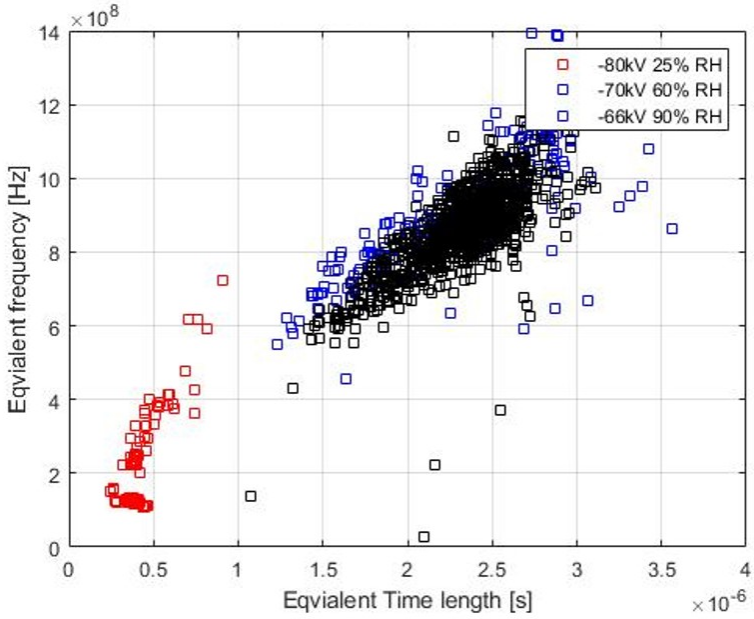

Fig. 5.9: TF map of PD signal of FRP test unit under different RH

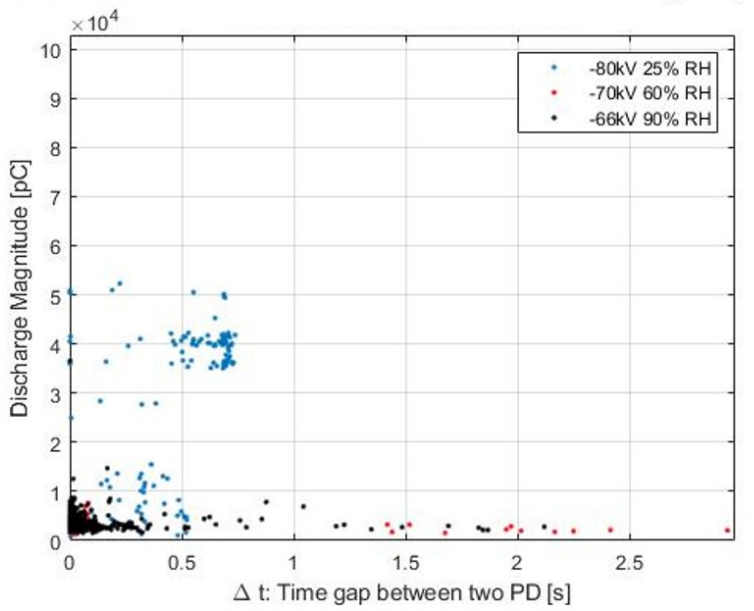

Fig. 5.10: Relationship of PD time gap and charge magnitude of FRP test unit under different RH

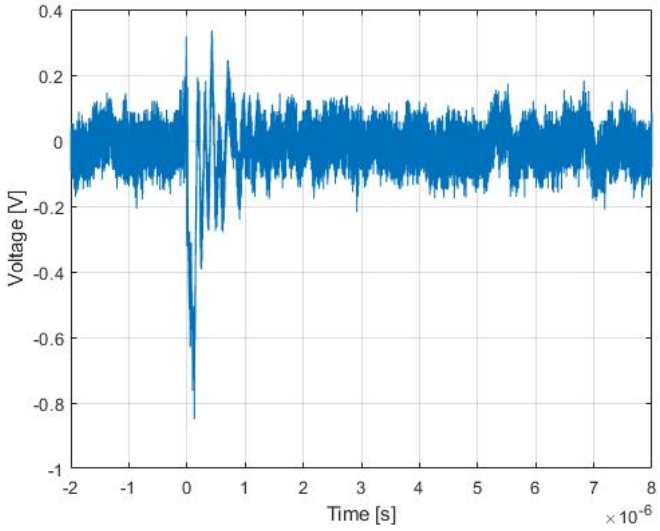

(a) Current with single PD pulse.

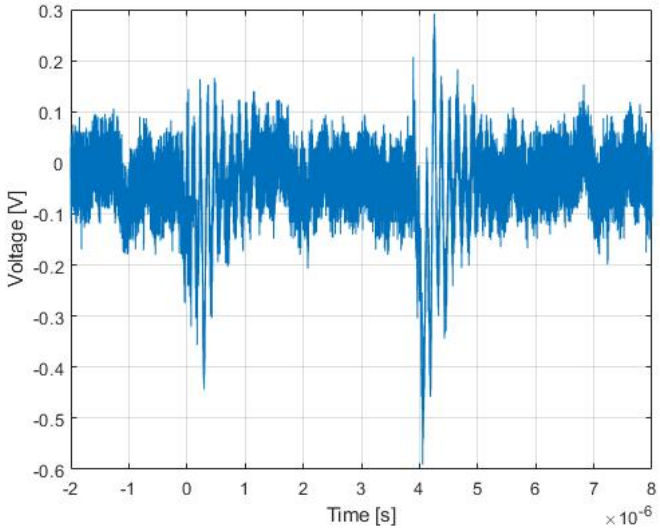

(b) Current with multiple PD pulses .

Fig. 5.11: PD leakage current from FRP sample PD tests under high RH levels.

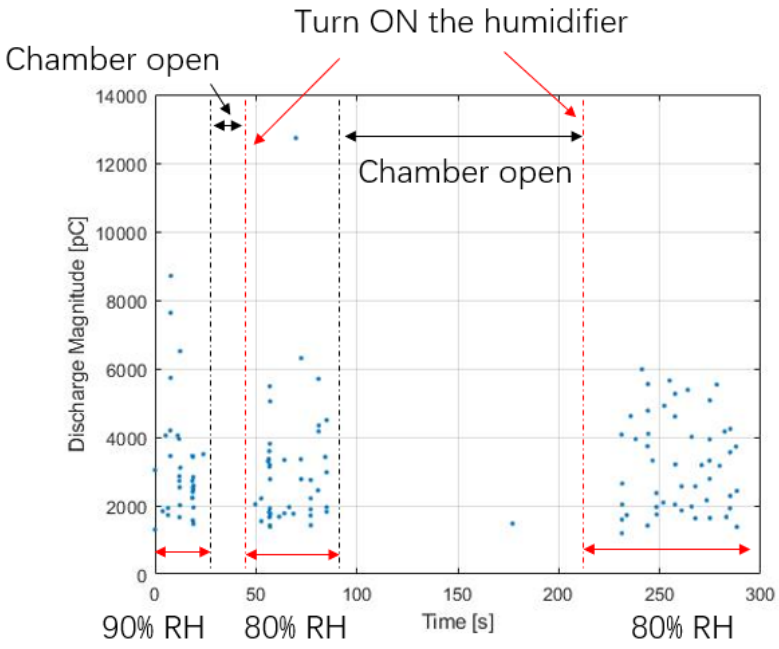

Fig. 5.12: Humidity influence test on PD activities of FRP test unit at -70kV

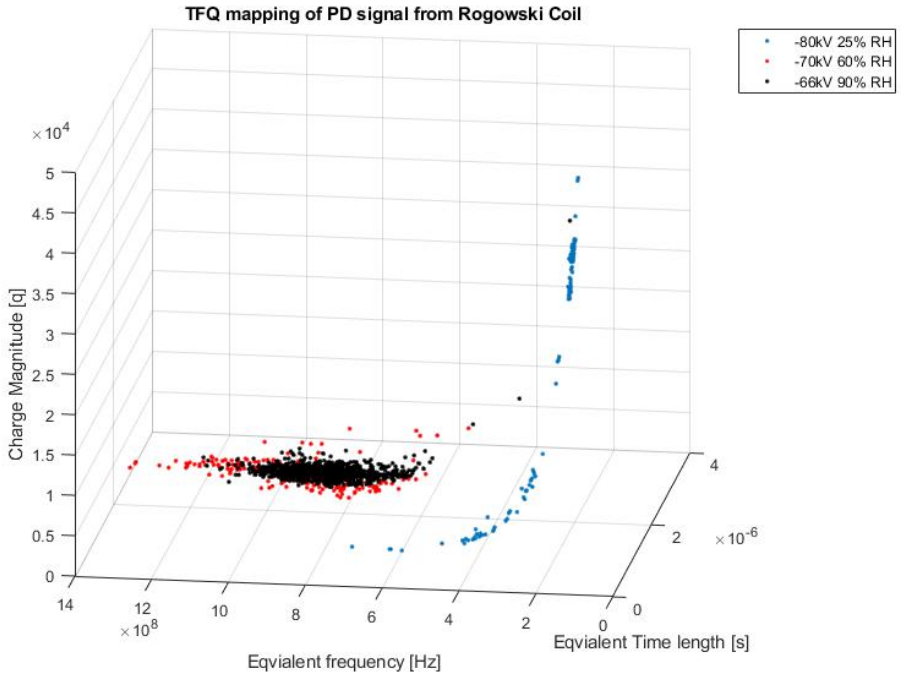

(a) 3D map.

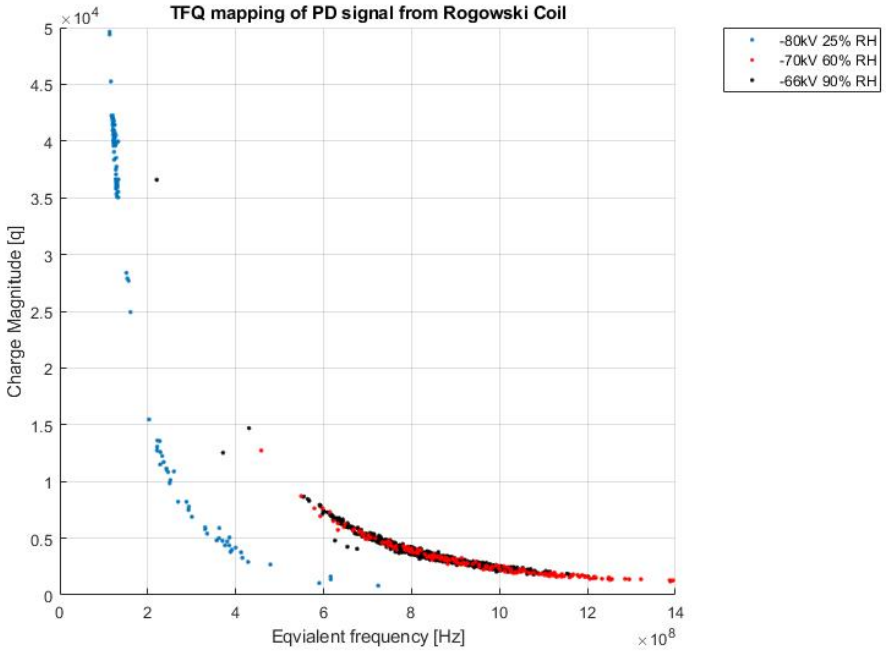

(b) Function of signal total charge magnitude Q and equivalent frequency F

Fig. 5.13: TFQ 3D map of PD signal of FRP test unit under different RH.

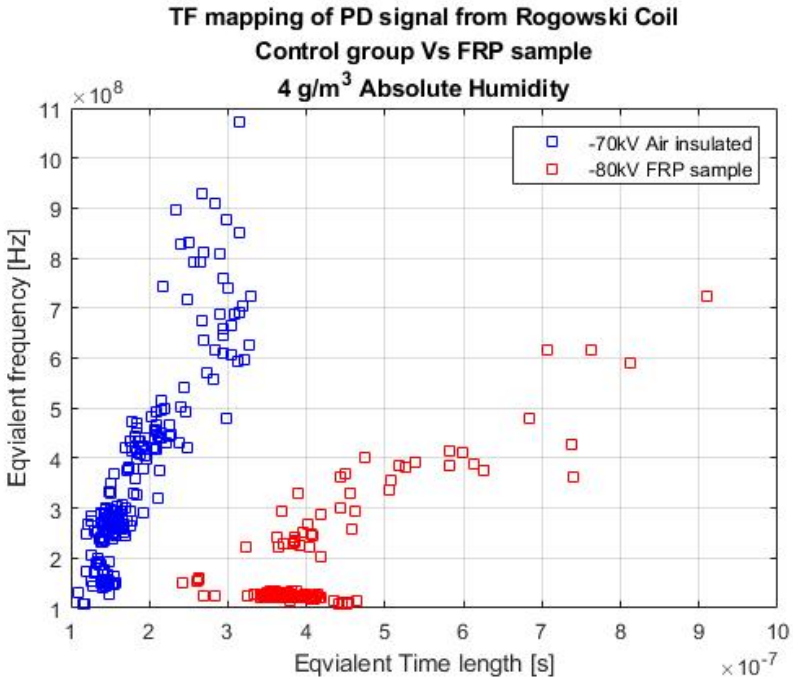

(a) 4 g/m^3 Absolute humidity.

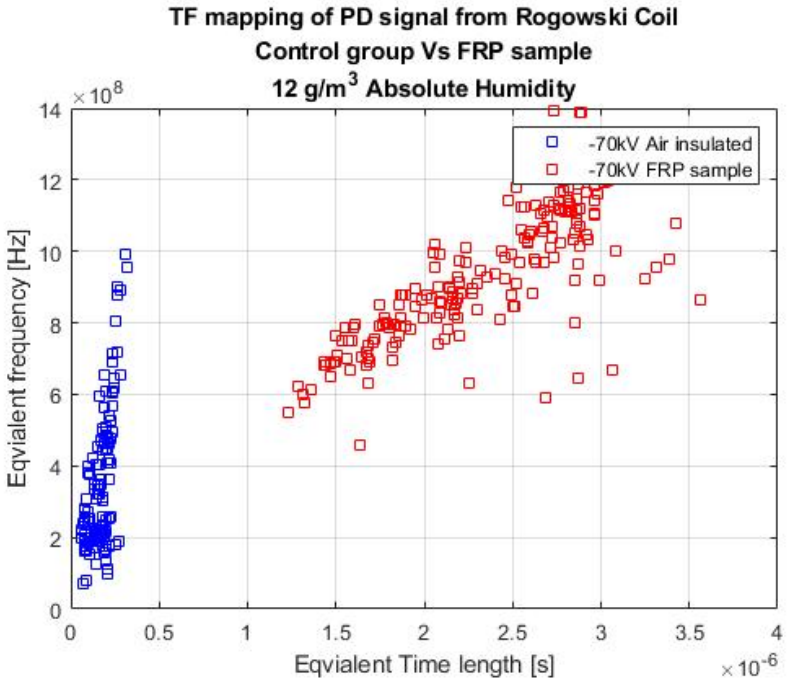

(b) 12 g/m^3 Absolute humidity.

Fig. 5.14: TF Map comparison of air insulated and FRP test unit under different absolute humidity level

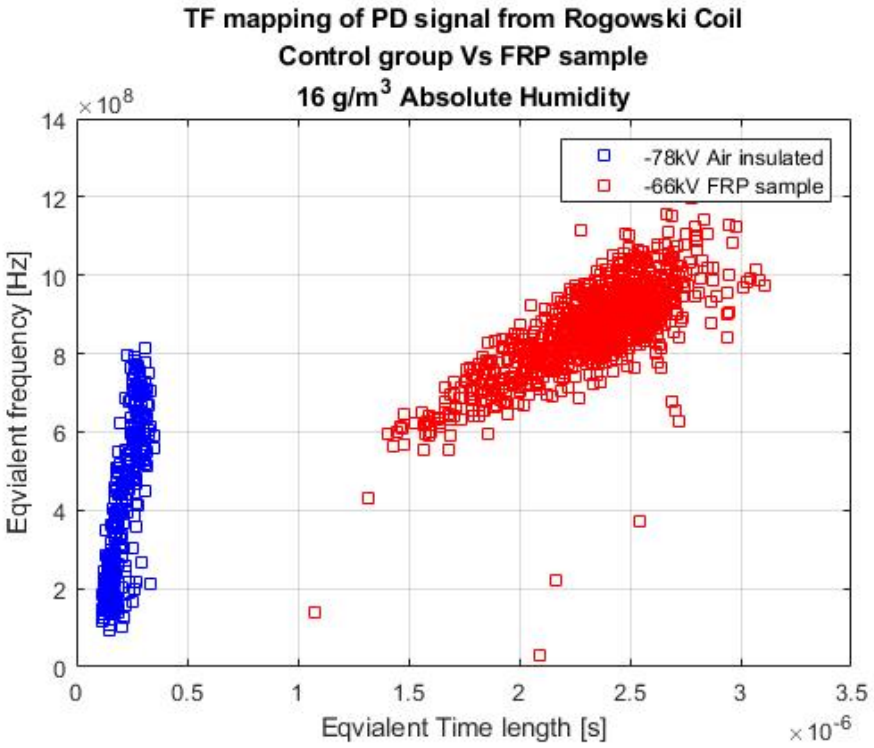

(c) 16 g/m^3 Absolute humidity.

Fig. 5.14: TF Map comparison of air insulated and FRP test unit under different absolute humidity level

Figure 5.14 shows the compared results of the air-insulated and FRP test unit under different absolute humidity levels. From the plot, we noticed that under the same absolute humidity level, the TF map results of the air-insulated and the FRP test unit can be easily separated by autocorrelation and K-Means clustering techniques, as per Section 2.4.2. When the environment's humidity level was low (below 8 g/m^3 absolute humidity), both the air-insulated and the FRP test unit's equivalent time lengths and equivalent frequencies were still very close to each other. When the environment's humidity level was high (above 12 g/m^3 absolute humidity), the leakage current of the FRP test unit changed to a small and low-frequency pulse cascaded with a high-frequency current signal, as per Figure 5.11. In the meantime, the leakage current of the air-insulated test unit did not change significantly. The change of leakage current characteristics made a gap between two signal clusters

larger in TF map systems.

5.1.4 Conclusion of HVDC PD Under Humidity Influence

Based on the test results described in section 5.1.1 and 5.1.2, we can conclude that:

- Humidity levels have a significant influence on PD activities.
    1. PD will be more activated in humid environmental conditions.
    2. The characteristics of PD pulses can be changed due to the change of humidity levels in the environment by changing the source of the PD.
- When the system is not air-insulated, like when using on FRP or silicon rubber as an insulator, the system's PDIV and flashover voltage will be significantly reduced due to the environment's increasing humidity levels.
- When the system is air-insulated, the system's PDIV will not be affected much due to the increased humidity levels in the environment. However, the flashover voltage will increase significantly when we increase the humidity level.

5.2 HVDC PD with Free Surface Charge Influence

The results of PD and flashover testing on the tested insulator samples with different polarity surface charges is presented and discussed below. To present the results, TF mapping, time and discharge magnitude model, and box plot figures are used.

Table 5.3 shows the PDIV and flashover voltage of the FRP test unit with a pre-stressing setup under positive, negative, and no surface charges. The temperature and relative humidity inside the chamber is 22°C and 35%RH. Since the experiment setup is symmetric, the source is only energized with negative voltage.

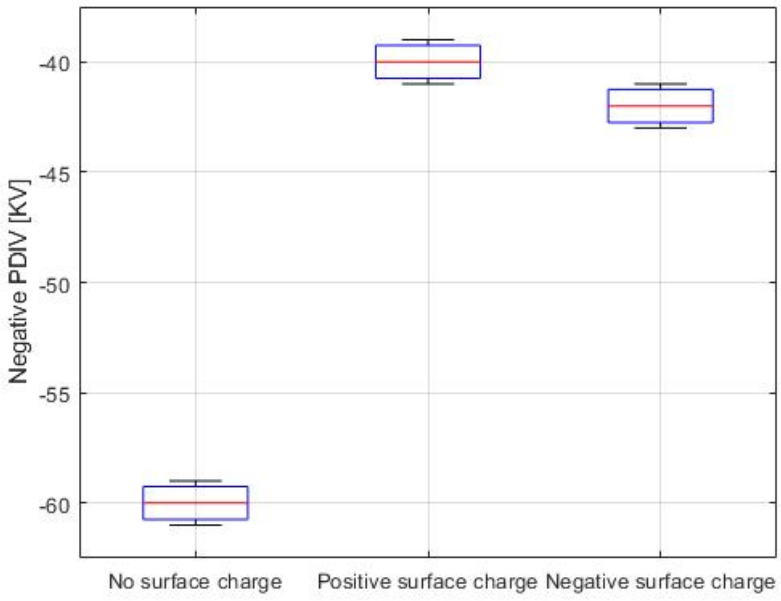

(a) Negative PDIV.

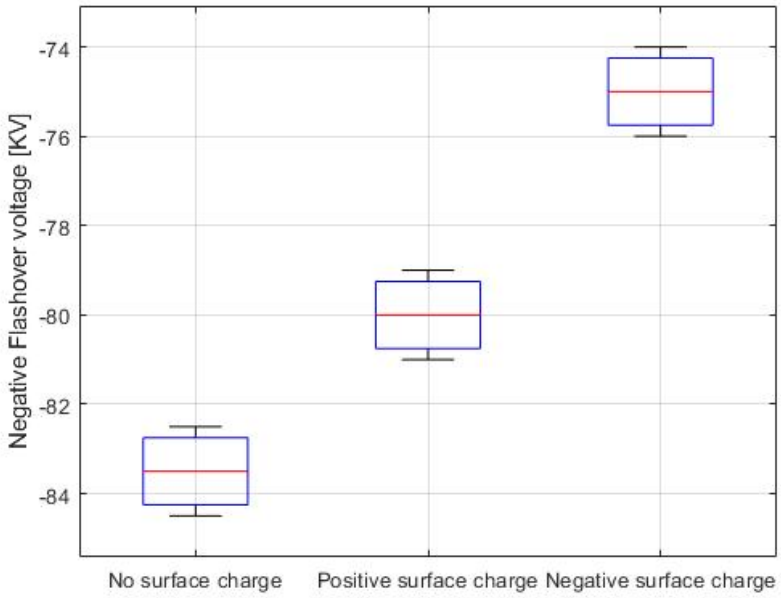

(b) Negative flashover.

Fig. 5.15: Boxplot of PDIV and flahsover voltage with surface charge influence.

Table 5.3: PDIV and Flash Over Voltage of FRP Unit with Surface Charges Influence.

Conditions	PDIV	Flashover voltage	Leakage current at PDIV
No surface charge	-60 kV	-83.5 kV	0.5 mA
Positive surface charge	-42 kV	-75 kV	0.2 mA
Negative surface charge	-40 kV	-80 kV	0.2 mA

The result shows that under the same test environment (temperature and humidity), surface charge (both positive and negative) on the insulator has a significant influence on PDIV. Both tests' PDIV reduced about 20 kV. On the other hand, the surface charge does not affect the system's flashover voltage much. When the surface charge and electrode voltage are the same polarities, the system's flashover voltage reduces about 3.5 kV. When the polarity of the surface charge and electrode voltage are different, flashover voltage reduces about 8.5 kV.

5.2.1 Result of FRP Test Unit Under Positive Surface Charge

During the positive surface charge test, we kept environmental parameters at 21°C and 35% humidity. By using the ring of needles, we inject free charge for 4 minutes at +20 kV level, we noticed that the PDIV of the system was −42 kV. Even though the PDIV was much lower than the FRP test without surface charge, the acquisition system didn't capture much PD pulses until −70 kV. The system flashover voltage is −75 kV.

5.2.2 Result of FRP Test Unit Under Negative Surface Charge

During the negative surface charge test, we kept environmental parameters at 21°C and 35% humidity. By using the ring of needles, we inject free charge for 4 minutes at −20 kV level, we were able to find out that the PDIV was reduced to −40 kV. However, the number of recorded PD pluses was very limited. We increased the source voltage to −50 kV and −70 kV, waited 10 mins at each level, and still limited PD pluses were captured by the acquisition system. When the source voltage was −78 kV, which is very close to the voltage level we set to capture PD pulses for the

FRP unit without surface charge, PD activities became much more activated. The system flashover voltage is -20 kV.

5.2.3 TF Map Result

Figure 5.16 shows the TF map result of the PD test of the FRP unit with positive, negative, and no surface charge.

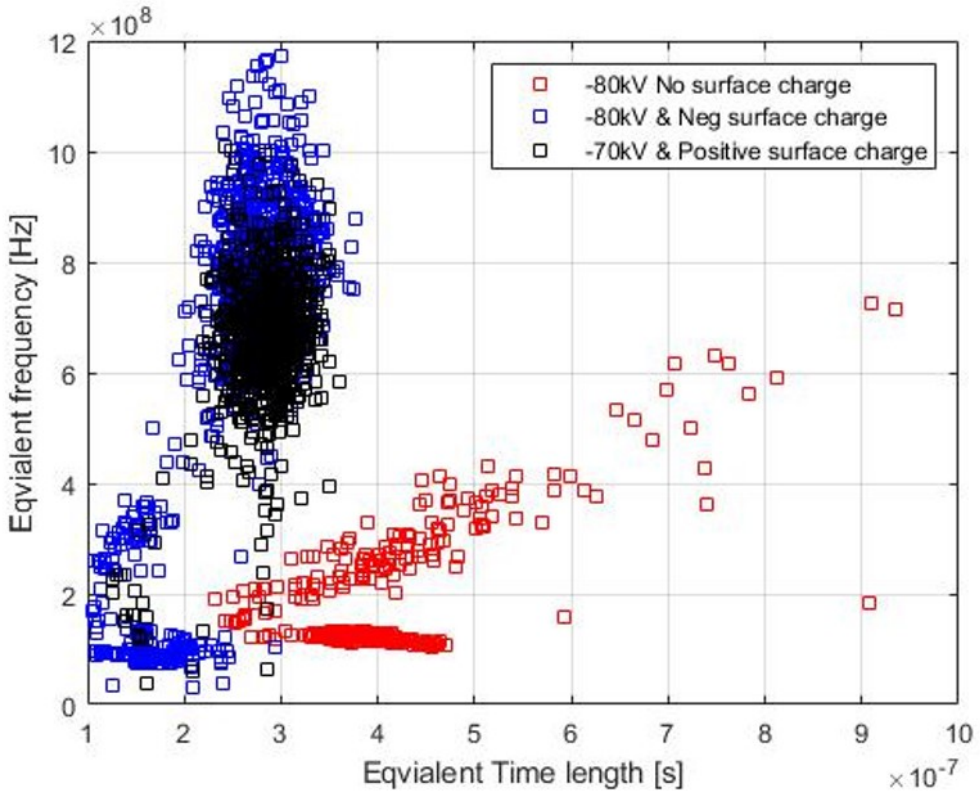

Fig. 5.16: TF map result of PD test of FRP unit with positive, negative and none surface charge.

From the influence of the surface charge existence, it can be noticed that in Figure 5.16, when a surface charge was injected onto the surface of the insulator, the projected data points (blue and black) on the TF map system was separated from the projected data points (red) from the test

without any surface charge. However, the pattern of projected data points on the TF map system was similar. It looks like when a surface charge was involved, the projected data points shifted to left a little on the two-dimensional plane.

From the influence of the surface charge polarity perspective, it can be noticed that in Figure 5.16, the projected data points from the positive surface charge test and negative surface charge test can be categorized in the same cluster.

5.2.4 TFQ 3D Map Result

Figure 5.17a is the TFQ 3D map result. With the PD pulse's total charge magnitude Q on the z axis, the 3D mapping system shows that when there is a surface charge involved in the test (positive or negative polarity), the location of projected data points on the 3D space is quite different from the test result without surface charge. However, all three test results follow a curve with exponential decay as the pulse's equivalent frequency increases, as per Figure 5.17b. The decay speed of the test with a surface charge present is faster than the test without surface charge. The decay curve of the test with positive and negative surface charges are almost identical.

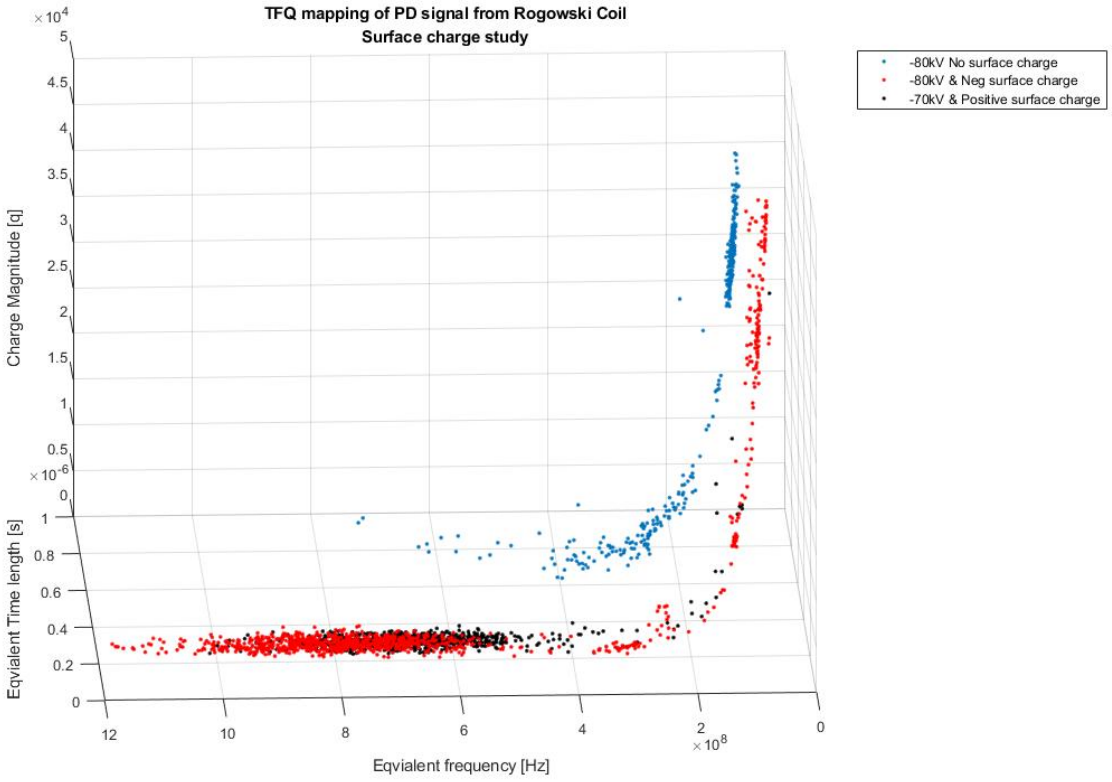

(a) 3D map.

Fig. 5.17: TFQ 3D map of PD signal of FRP test unit with positive, negative and none surface charge.

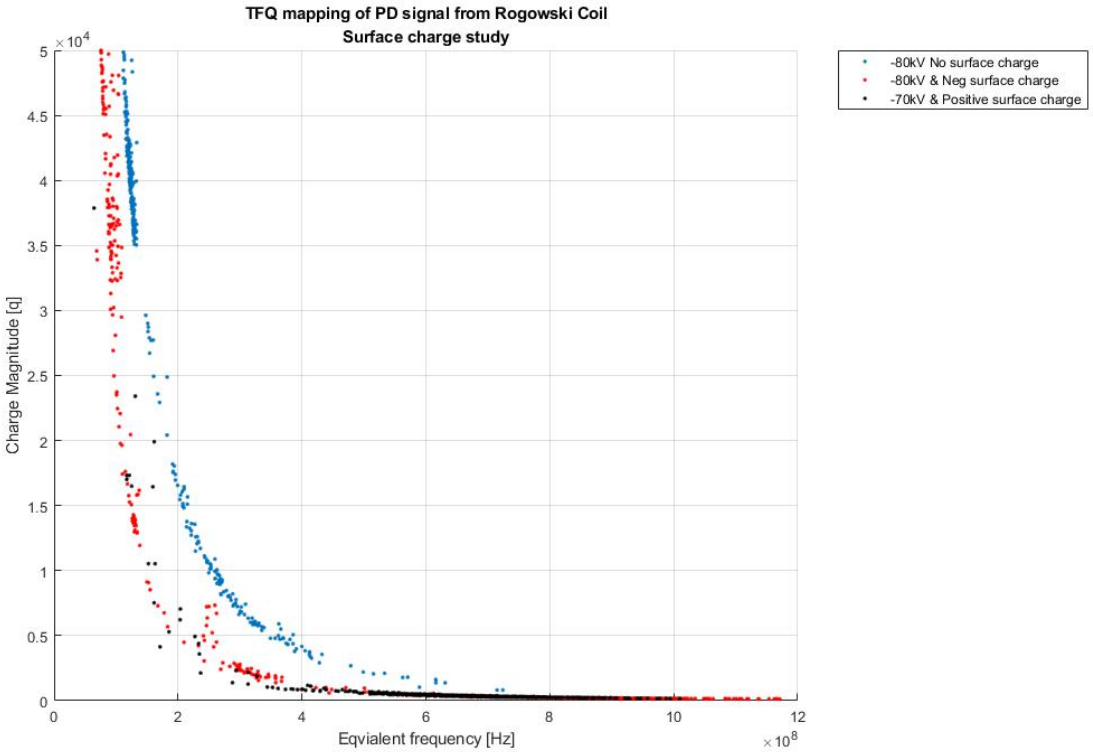

(b) Function of signal total charge magnitude Q and equivalent Frequency F

Fig. 5.17: TFQ 3D map of PD signal of FRP test unit with positive, negative and none surface charge.

5.2.5 Conclusion of HVDC PD Under Free Surface Charge Influence

Based on the test results described in section 5.2, we can conclude that:

- Free charge on the insulator surface has significant influence on PD activities.

  1. Free charge on the insulator surface will reduce the PDIV and flashover voltage of the system.
  2. The system's PDIV and flashover with positive surface charges present are lower than when negative surface charges were present while the electrode was energized with negative DC

voltage.

- On the TF map system, the projected data points from the test unit with surface charge were separated from the projected data points of the test unit without surface charge.
- On the TFQ 3D map system, the projected data points from the test unit with surface charge were also separated from the projected data points of the test unit without surface charge.
- On the TFQ 3D map system, the YZ plane presents a function between signal total charge magnitude Q and equivalent frequency F. From the test result, the function follows a curve with exponential decay. The decay speed is faster when the surface charge is present.

5.3 Summary

The test results demonstrated that both the humidity and the free charge on the insulator surface have a significant influence on the partial discharge activities for the given electrode configuration. Regardless of the system configuration, as the humidity level increases, the PD repetition rate increases as well. Under tested electrode configurations (air insulted and FRP), humidity can affect the system's PDIV and flashover voltage as well, but a much stronger impact was observed on FRP test configurations. We believe that when the insulator is installed, ions are attracted, trapped, and form an ionization zone on the surface of the insulator. However, the thickness of this ionization zone diminishes as the humidity level increases [11] and forms a higher electric field inside the zone. Therefore, the PDIV decreases with the increase in humidity. Moreover, the test results show that the leakage current characteristics changes with the increase of humidity.

The test results also demonstrated that PDIV and flashover voltage are directly affected by the free charge on the insulator surface. When surface charges are present, regardless of the charge's polarity, the PDIV of the tested electrode configuration reduced about 20 kV. When the surface charge is positive, the negative flashover voltage drops about 10 kV. But when the surface charge is negative, the negative flashover voltage only drops about 4 kV. From the test results, there is no evidence to show that PD repetition rates can be affected by the presence of surface charge.

Through the PD identification process, we noticed that when the system is involved in humidity or surface charge effects, the plusses can be identified by projecting the signal on TF or TFQ map system. Moreover, on the TFQ 3D map system, the results show that the relationship between signal total charge magnitude Q and equivalent frequency F follows a curve with exponential decay. When the system was under a high humidity environment or with surface charge present, the decay speed was faster than normal conditions.

Chapter 6

Conclusions and Future Work

6.1 Conclusion

After the three field tests at a HVDC substation were conducted, we found that the discharge phenomena were only brought to attention when specific conditions were met, making them able to be heard or have arcing visible to the naked eye. By measuring the leakage current and electric field around the smoothing reactor, we noticed that the leakage current from the insulator posts is periodic and comes from switching behavior in the converter station. However, only some random partial discharge pluses can be captured by our electric field probe. These partial discharge pluses were purely random and only appear under certain weather conditions. We believe the partial discharge occurring on the insulator stacks is a result of static charge buildup on the insulator sheds (no environmental pollution). When the humidity is high, the static charge buildup on the insulator will spread along the insulator surface and create a conducting path between the smoothing reactor, flange, and ground. Since the flange is floating metal within this conducting path, the sharp edge of the flange will generate corona and cause discharge problems.

A scaled-down model with a fog chamber was built in the University's High Voltage Lab to study the relationship between the partial discharge activities and environmental influences. Two

different studies (humidity and surface charge) were applied on air and FRP insulated HVDC system in order to get a better understanding of the environmental influences on partial discharge behaviours. The experiment result demonstrated that for the given electrode configuration, both humidity and surface charge have a significant effect on the behaviour of partial discharge. The PD repetition rate is directly affected by the increase in humidity levels inside the fog chamber. When the system is air-insulated, the test system's PDIV was not affected much by increasing the humidity level while the flashover voltage was significantly increased. When the solid insulator (FRP, SIR) was installed between electrodes, the test system's PDIV significantly decreased either the increment of humidity inside the chamber or surface charge present. However, the flashover voltage was only affected by the humidity level; the presence of a surface charge on the insulator only had a minor effect on flashover voltage. Section 5.1.1 and 5.1.2 demonstrated that current-voltage characteristics of the PD pulses were also significantly affected by the humidity changes. Figures 5.5, 5.13, and 5.17 show that among all our tests, the function between signal total charge magnitude Q and equivalent frequency F follows a curve with exponential decay. Also, these figures show that when the system was under a high humidity environment or with surface charge presents, the decay speed is faster than normal conditions.

By connecting the field test and lab test result, we believe that the combination of high humidity levels and free static charge along the insulator of the smoothing reactor triggered the random discharge phenomena at the HVDC substation. Both moisture and surface charges have significant effects on the system's PDIV. With the presence of moisture and surface charge, the dielectric strength of air around the insulator flange was significantly reduced. Thus, random corona and small sparks were observed under specific weather conditions. What's more, the PD repetition rate is directly affected by the increase in humidity levels, and that is why most of the discharge phenomena were reported in early spring.

The best solutions for reducing discharge phenomena at the substation are as follows. First, install a corona ring between the insulator's flange. A corona ring distributes the electric field

gradient and lowers its maximum values below the corona threshold. Second, apply a dielectric coating on the insulator's flange. An insulating layer on top of the metal can prevent partial discharge from happening on the flange's sharp edge.

6.2 Future Work

In this thesis, the measurement results demonstrated that for the given electrode configuration, both humidity and surface charges have significant effects on the behaviour of the partial discharge. In this section, further studies are proposed for improving the accuracy of the test results and building a stronger correlation between partial discharge and environmental influences.

- Future work should be carried out to determine the effects of light pollution (salt contamination) and the icing on the partial discharge and flashover characteristics of the insulation system.
- Perform PDIV and flashover tests on SIR insulator samples with different polarity surface charges present.
- Investigate the dimension of insulator changes with environmental influences (Humidity and surface charge).
- Investigate the PD pulse's current-voltage characteristics changes affected by the change of humidity levels.
- Investigate the PD phenomenon when de-energizing the energized HVDC test unit.
- Future work should be carried out to study the exponential decay function between signal total charge magnitude Q and equivalent frequency F, described in Chapter 5.
- Future work should be carried out to determine if a corona ring can improve the PD phenomenon under high-level humidity environments or with the presence of surface charges.

- Future work should be carried out on the substation to install a long-term based data acquisition system for collecting leakage current and electric field information.

References

[1] C. Xiaoxuan, G. Ruifeng, and Z. Jie, "Study for Arrangement of the Smoothing Reactor in ± 800kV UHVDC Project," *International Conference on High Voltage Engineering and Application*, pp. 371–374, 2008.

[2] T. Chen, J. Cao, G. Zhou, Y. Wang, and X. Wen, "Electric Field Research of ± 800kV Dry-type Smoothing Reactor," *International Conference on Electrical Machines and Systems*, pp. 1484–1487, 2014.

[3] Y. Li, Q. Zhang, M. Gao, H. Ni, Y. Zhao, G. Liu, and K. Wang, "Influence of fiber impurities on dc partial discharge process in oil-pressboard insulation," in *2017 IEEE 19th International Conference on Dielectric Liquids (ICDL)*, June 2017, pp. 1–5.

[4] J. S. Pearson, O. Farish, B. F. Hampton, M. D. Judd, D. Templeton, B. W. Pryor, and I. M. Welch, "Partial discharge diagnostics for gas insulated substations," *IEEE Transactions on Dielectrics and Electrical Insulation*, vol. 2, no. 5, pp. 893–905, Oct 1995.

[5] M. Amer, J. Laninga, W. McDermid, D. R. Swatek, and B. Kordi, "Surface charging and its effects on DC flashover strength of insulating materials," *IEEE Transactions on Dielectrics and Electrical Insulation*, vol. 25, no. 6, pp. 2452–2460, Dec 2018.

[6] IEC 60270, "High-voltage test techniques - Partial discharge measurements," *Tech. Rep.*, 2001.

[7] T. Byrne, "Humidity effects in substations," *11th Petroleum and Chemical Industry Conference Europe Electrical and Instrumentation Applications, PCIC 2014*, pp. 1–10, 2014.

[8] X. Zhang, X. Bian, X. Cui, T. Lu, H. Li, Q. Li, Y. Zhu, and A. E. Platform, "Experimental Investigation on Humidity Effects on the Variations of Positive DC Corona Discharge," *2016 IEEE International Power Modulator and High Voltage Conference (IPMHVC)*, pp. 598–602, 2016.

[9] J. J. Smit, "Partial Discharges at dc Voltage : Their Mechanism, Detection and Analysis," *IEEE Transactions on Dielectrics and Electrical Insulation*, vol. 12, pp. 328–340, April 2005.

[10] D. Wienold, U. Lühring, and F. Jenau, "Detection and distinction of partial discharges in air at DC voltage by using a non-conventional approach in the high-frequency range," *IEEE Industrial and Commercial Power Systems Europe*, no. 03, 2017.

[11] M. Nakano and A. Mizuno, "Influence of humidity on charge density and electric field in electrostatic precipitators," *Journal of Physics D: Applied Physics*, 1992.

[12] W. Mcdermid and T. Black, "Experience with Preventing External Flashovers in HVDC Converter Stations," *2008 IEEE International Symposium on Electrical Insulation*, pp. 81–84, 2008.

[13] K. Wang, R. Liao, L. Yang, J. Li, S. Grzybowski, and J. Hao, "Optimal features selected by NSGA-II for partial discharge pulses separation based on time-frequency representation and matrix decomposition," *IEEE Transactions on Dielectrics and Electrical Insulation*, vol. 20, no. 3, pp. 825–838, June 2013.

[14] C. Zhang, L. Wang, and Z. Guan, "Pollution Flashover Performance of Full-scale ± 800 kV Converter Station Post Insulators at High Altitude Area," *IEEE Transactions on Dielectrics and Electrical Insulation*, vol. 20, no. 3, June 2013.

[15] C. Zhang and L. Wang, "Investigation of DC Discharge Behavior of Polluted Porcelain Post Insulator in Artificial Rain," *IEEE Transactions on Dielectrics and Electrical Insulation*, vol. 23, no. 1, pp. 331–338, February 2016.

[16] F. Guastavino, A. Bruzzone, C. Gianoglio, and E. Torello, "Influence of DC Component on Partial Discharge Activity," *Conference on Electrical Insulation and Dielectric Phenomena, CEIDP*, vol. 2018-Octob, pp. 535–537, 2018.

[17] H. Saadati, P. Werle, J. M. Seifert, E. Gockenbach, and H. Borsi, "Fundamental Difference of Partial Discharge Phenomena under AC and DC Stresses," *ICHVE 2018 - 2018 IEEE International Conference on High Voltage Engineering and Application*, pp. 1–4, 2019.

[18] H. V. Nguyen, B. T. Phung, and T. Blackburn, "Effect of temperatures on very low frequency partial discharge diagnostics," *Proceedings of the IEEE International Conference on Properties and Applications of Dielectric Materials*, vol. 2015-Octob, pp. 272–275, 2015.

[19] L. Mariut, "Temperature gradient effect on partial discharge activity-modelling and simulation," *2012 International Conference on Applied and Theoretical Electricity, ICATE 2012 - Proceedings*, pp. 1–8, 2012.

[20] Suwarno and H. Sutikno, "Effects of temperature on the breakdown voltage and partial discharge patterns of biodegradable oil," *Proceedings of the 2011 International Conference on Electrical Engineering and Informatics, ICEEI 2011*, no. July, pp. 1–6, 2011.

[21] T. Han, J. G. Su, T. T. Ma, F. Y. Wang, Y. Q. Xing, and Y. Gao, "Partial Discharge Characteristics during Treeing Process in Silicone Rubber at 20 and-100 °C," *IEEE Transactions on Applied Superconductivity*, vol. 29, no. 2, March 2019.

[22] L. Hui, S. Qinghe, Y. Jun, and M. Hailei, "Detection and processing for ±660 composite insulator abnormal discharge," *2014 International Conference on Power System Technology*, pp. 1404–1409, Oct 2014.

[23] F. Meng, X. Zhang, X. Wu, and B. Xu, "Experimental studies on air humidity affecting partial discharge in switchgear," pp. 1237–1241, Oct 2013.

[24] X. Wang and C. You, "Effect of Humidity on Negative Corona Discharge of Electrostatic Precipitators," *IEEE Transactions on Dielectrics and Electrical Insulation*, vol. 20, pp. 1720–1726, May 2013.

[25] E. Lemke, P. Schmiegel, and W. Mosch, "PD Phenomena on Dielectric Surfaces under dc Stresses Influenced by Air Humidity," *IEEE Transactions on Electrical Insulation*, vol. 26, no. 3, pp. 453–457, Jun 1991.

[26] R. Soltani, E. David, and L. Lamarre, "Study on the effect of humidity on dielectric response and partial discharges activity of machine insulation materials," *2009 IEEE Electrical Insulation Conference, EIC 2009*, pp. 343–347, June 2009.

[27] Z. Nawawi, Y. Murakami, N. Hozumi, and M. Nagao, "Effect of humidity on time lag of partial discharge in insulation-gap-insulation system," pp. 199–203, June 2006.

[28] U. Lühring, D. Wienold, and F. Jenau, "Influence of humidity on pulse shape parameters of positive corona discharges in air at DC voltage," *Conference Proceedings - 2017 17th IEEE International Conference on Environment and Electrical Engineering and 2017 1st IEEE Industrial and Commercial Power Systems Europe, EEEIC / I and CPS Europe 2017*, no. 03, 2017.

[29] R. Kubota, T. Kawashima, Y. Murakami, and M. Nagao, "Partial Discharge Inception Voltage under Surge Voltage Application Influenced by Surface Charge on Insulating Sheet," *2016 IEEE Conference on Electrical Insulation and Dielectric Phenomena (CEIDP)*, pp. 171–174, 2016.

[30] K. Takabayashi, R. Nakane, H. Okubo, and K. Kato, "High Voltage DC Partial Discharge and Flashover Characteristics with Surface Charging on Solid Insulators in Air," *IEEE Electrical Insulation Magazine*, vol. 34, pp. 18–26, 2018.

[31] B. X. Du and M. Xiao, "Influence of surface charge on dc flashover characteristics of epoxy/bn nanocomposites," *IEEE Transactions on Dielectrics and Electrical Insulation*, vol. 21, no. 2, pp. 529–536, April 2014.

[32] S. Kumara, Y. Serdyuk, and S. Gubanski, "Simulation of surface charge effect on impulse flashover characteristics of outdoor polymeric insulators," *IEEE Transactions on Dielectrics and Electrical Insulation*, vol. 17, no. 6, pp. 1754–1763, Dec 2010.

[33] U. Fromm, "Interpretation of Partial Discharges at dc Voltages," *IEEE Transactions on Dielectrics and Electrical Insulation*, vol. 2, no. 5, Oct 1995.

[34] S. Wenrong, L. Junhao, Y. Peng, and L. Yanming, "Digital detection, grouping and classification of partial discharge signals at DC voltage," *IEEE Transactions on Dielectrics and Electrical Insulation*, vol. 15, no. 6, pp. 1663–1674, Dec 2008.

[35] N. C. Sahoo, M. M. Salama, and R. Bartnikas, "Trends in partial discharge pattern classification: A survey," *IEEE Transactions on Dielectrics and Electrical Insulation*, vol. 12, no. 2, pp. 248–264, May 2005.

[36] H. Janani and B. Kordi, "Towards automated statistical partial discharge source classification using pattern recognition techniques," *IET High Voltage*, vol. 3, no. 3, pp. 162–169, July 2018.

[37] H.-g. Kranz and R. Krump, "Partial discharge diagnosis using statistical optimization on a PC-based system," *IEEE Transactions on Dielectric and Electrical Insulation*, vol. 2, no. 1, pp. 93–98, Feb 1992.

[38] M. M. A. Salama and R. Bartnikas, "Determination of neural-network topology for partial discharge pulse pattern recognition," *IEEE Transactions on Neural Networks*, vol. 13, no. 2, pp. 446–456, March 2002.

[39] A. Contin, A. Cavallini, G. C. Montanari, G. Pasini, and F. Puletti, "Digital detection and fuzzy classification of partial discharge signals," *IEEE Transactions on Dielectrics and Electrical Insulation*, vol. 9, no. 3, pp. 335–348, Aug 2002.

[40] H. Ma, J. C. Chan, T. K. Saha, and C. Ekanayake, "Pattern recognition techniques and their applications for automatic classification of artificial partial discharge sources," *IEEE Transactions on Dielectrics and Electrical Insulation*, vol. 20, no. 2, pp. 468–478, April 2013.

[41] A. Contin and S. Pastore, "Classification and separation of partial discharge signals by means of their auto-correlation function evaluation," *IEEE Transactions on Dielectrics and Electrical Insulation*, vol. 16, no. 6, pp. 1609–1622, Aug 2009.

[42] L. Hao, P. L. Lewin, J. A. Hunter, and D. J. Swaffield, "Discrimination of Multiple PD Sources Using Wavelet Decomposition and Principal Component Analysis," *IEEE Transactions on Dielectrics and Electrical Insulation*, vol. 18, no. March 2011, pp. 1702–1711, 2011.

[43] A. Graps, "An Introduction to Wavelets," *IEEE Computational Science and Engineering*, vol. 2, no. 2, pp. 50–61, Summer 1995.

[44] A. Krivda, "Recognition of discharges: Discrimination and classification," *Delft University Press*, 1995.

[45] J. A. Ardila-Rey, J. M. Martínez-Tarifa, G. Robles, and M. V. Rojas-Moreno, "Partial discharge and noise separation by means of spectral-power clustering techniques," *IEEE Transactions on Dielectrics and Electrical Insulation*, vol. 20, no. 4, pp. 1436–1443, August 2013.

[46] J. M. Fresno, J. A. Ardila-Rey, J. M. Martínez-Tarifa, and G. Robles, "Partial discharges and noise separation using spectral power ratios and genetic algorithms," *IEEE Transactions on Dielectrics and Electrical Insulation*, vol. 24, no. 1, pp. 31–38, Feb 2017.

[47] J. C. Chan, H. Ma, and T. K. Saha, "Time-frequency sparsity map on automatic partial discharge sources separation for power transformer condition assessment," *IEEE Transactions on Dielectrics and Electrical Insulation*, vol. 22, no. 4, pp. 2271–2283, Aug 2015.

[48] R. E. James and B. T. Phung, "Development of computer-based measurements and their application to PD pattern analysis," *IEEE Transactions on Dielectrics and Electrical Insulation*, vol. 2, no. 5, pp. 838–856, Oct 1995.

[49] A. Cavallini, G. C. Montanari, F. Puletti, and A. Contin, "A new methodology for the identification of PD in electrical apparatus: Properties and applications," *IEEE Transactions on Dielectrics and Electrical Insulation*, vol. 12, no. 2, pp. 203–215, May 2005.

[50] U. Fromm and P. H. F. Morshuis, "Partial discharge classification at dc voltage," in *Proceedings of 1995 IEEE 5th International Conference on Conduction and Breakdown in Solid Dielectrics*, July 1995, pp. 403–407.

[51] P. Morshuis, M. Jeroense, and J. Beyer, "Partial discharge. part xxiv: The analysis of pd in hvdc equipment," *IEEE Electrical Insulation Magazine*, vol. 13, no. 2, pp. 6–16, March 1997.

[52] P. H. F. Morshuis and J. J. Smit, "Partial discharges at dc voltage: their mechanism, detection and analysis," *IEEE Transactions on Dielectrics and Electrical Insulation*, vol. 12, no. 2, pp. 328–340, April 2005.

[53] N. D. Perera, "Detection, Localization, and Recognition of Faults in Transmission Networks Using Transient Currents," *PhD Thesis of University of Manitoba*, 2012.

[54] H. de O. Mota, F. Vasconcelos, and R. da Silva, "Real-time wavelet transform algorithms for the processing of continuous streams of data," *IEEE International Workshop on Intelligent Signal Processing, 2005.*, pp. 346–351, 2006.

[55] R. S. Pathak, *The Wavelet transform*, 1st ed., C. Chui, Ed. Atlantis Press, 2009.

[56] S. N. Fernando, "Investigation of application of wavelets to detect minor insulation failures during impulse tests on power transformers," *PhD Thesis of University of Manitoba*, August 2008.

[57] H. D. O. Mota, F. H. Vasconcelos, and R. M. Da Silva, "Real-time wavelet transform algorithms for the processing of continuous streams of data," *2005 IEEE International Workshop on Intelligent Signal Processing - Proceedings*, pp. 346–351, 2005.

[58] Y. Sheng, "Wavelet Trasform," in *Elecetical Engineering handbook*, 2010.

[59] S. G. Mallat, "A theory for multiresolution signal decomposition: The wavelet representation," *Fundamental Papers in Wavelet Theory*, vol. I, no. 7, pp. 494–513, 2009.

[60] H. H. Giv, "Directional short-time fourier transform," *Journal of Mathematical Analysis and Applications*, vol. 399, no. 1, pp. 100,107, 2013-03-01.

[61] W. Lu and Q. Zhang, "Deconvolutive short-time fourier transform spectrogram," *IEEE Signal Processing Letters*, vol. 16, no. 7, pp. 576–579, July 2009.

Appendix A

Signal Processing Techniques Used in Project

A.1 Wavelet Theory

A wavelet is mathematical function which is widely used in signal processing and image compression. What does wavelet do is divide a given function into different frequency components and study each component with resolution matches its scale [43]. Based on this characteristic, the most common function of wavelet is to recover weak signal from noise. This section will briefly explain wavelet transforms and wavelet denoising method for PD signals.

A.1.1 Wavelet Transforms

Wavelet transform represents a time limited signal as a weighted sum of orthogonal functions which can be obtained by suitably scaling and translating from a 'mother' [53]. This procedure can help reduced information which required to present a transient and help to cut wavelet coefficients when justify the disturbance type [54–56]. A mother wavelet function is defined as a finite-length or fast-decaying oscillating waveform and it must have zero average, as in the examples shown in Fig. A.1:

The following two sections (2.3.1.1 and 2.3.1.2) will briefly describe the continuous wavelet transform (CWT) and the discreated wavelet transform (DWT) which are the wavelet transforms

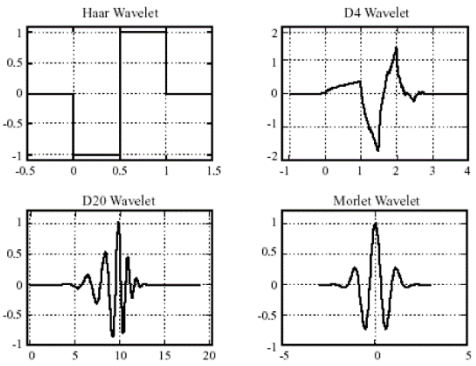

Fig. A.1: Example of common mother wavelets [53], [57].

will be implemented in my experiment.

A.1.1.1 Continuous Wavelet Transformation

Continuous wavelet transformation is wavelet transformation which letting the translation and scale parameter of the wavelets vary continuously. The result of CWT is to provides an overcomplete representation of analyzed signal. What does CWT do is apply a scale (α) and a time shift (τ) to a target signal in time domain so it will transfer into a two-dimensional function which represents the signal in the time scale space and is referred to as joint time-scale representation [54–56]. This technic is widely used in the analysis of non-stationary and fast transient signals [55, 56]. CWT is defined as

$$CWT_x(\tau, a) = \frac{1}{\sqrt{|a|}} * \int x(t)\varphi\left(\frac{t-\tau}{a}\right) dt \tag{A.1}$$

φ must satisfies:

$$\int \varphi dt = 0 \tag{A.2}$$

Where a is the scale factor and τ is the translation factor. However, we usually consider only

positive factor $\alpha > 0$. The wavelets are dilated when the scale factor $\alpha > 1$ and are contracted when $\alpha < 1$. The wavelet,$\varphi(\alpha, \tau)(t)$, generated from the same basic wavelet by applying different scale, α , and location τ , however the transformation result will all have same shape.

A.1.1.2 Discreate wavelet transform

The CWT transfer a one-dimensional time signal to a joint representation of two-dimensional time-scales function and the time bandwidth product of the CWT output isthe square of that of the signal . However, in most of signal processing's case, we want to represent the target signal efficiently with fewer parameters. Thus, the discreate wavelet transform (DWT) is introduced in signal processing due to its capability of reducing the time bandwidth product of the WT output. The term discreate wavelet transform means apply discrete scale and translation factors to the continuous wavelets. The discreate scale is expressed as a = a_0^i, where i is integer and $a_0 > 1$ is a fixed dilation step [58]. The discreate translation factor is expressed as $\tau = k\tau_0 a_0^i$, where k is an integer [58]. The translation depends on the dilation step, a_0^i. The corresponding discrete wavelets are written as:

$$DWT_x(\tau, a) = \frac{1}{\sqrt{|a|}} \sum x(k)\varphi\left(\frac{k - na_0^m\tau_0}{a_0^m}\right) \tag{A.3}$$

By careful selection of τ_0 and a_0, the family of scaled and shifted mother wavelets constitutes an orthonormal basis [25]. For example, when we select $a_0 = 2, \tau_0 = 1$ to constitute the orthonormal basis, the decomposed signals won't have any information redundancies, this property is called dyadic orthonormal property [55,56,58,59]. What's more, with this choice of a_0 and τ_0, there exists a novel algorithm, known as Multiresolution Signal Decomposition technique [59], to decompose a signal into scales with different time and frequency resolution.

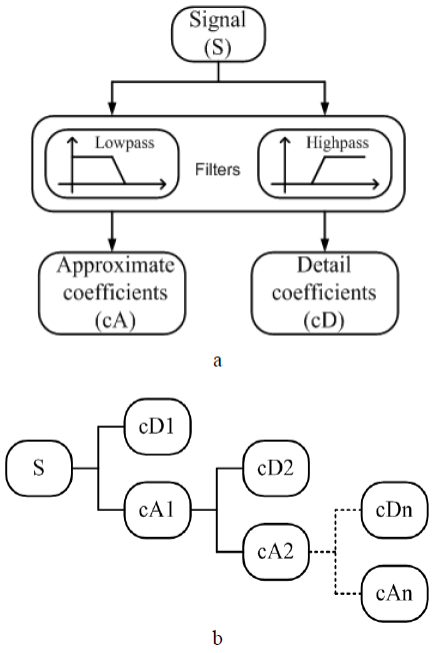

Fig. A.2: Wavelet denoising procedure for PD signals [42].

A.1.2 Wavelet denoising method for PD signals

Wavelet decomposition also known as Optimal Subband Tree Structuring (SB-TS) is a wavelet transform where the discrete-time (sampled) signal is passed through several filters [42]. The advantage of this procedure is it can provide information about original signals in both time and frequency domain within specific frequency ranges [42]. Due to this property, WD is widely applied in signal denoising filed to remove unrelated noises.

The wavelet decomposition process acts as a pair of complementary high-pass and low-pass filters which decompose the original signal (S) into a series of detail (D) and approximate (A) coefficients respectively, as shown in Figure A.2 a. The operation of the transform is an iterative process where the approximation coefficients are used as the new input for the next decomposition level which is shown in Figure A.2 b. Within the schematic, cAi and cDi represent the approximate and detail decomposition coefficients and I denotes the decomposition level. The original signal can

be decomposed into user-defined number of levels. Each level is half the bandwidth (sampling rate in frequency domain) and half the length (sample number in time domain) than the previous level. The operation of this analysis tool effectively characterizes the original signal at various frequency ranges that are then represented by coefficients at each node of the decomposition tree.

A.2 Short Time Fourier Transform (STFT)

The Fourier transform is widely used in signal analysis and processing. When dealing with periodic signals, the Fourier coefficients can decay very fast, especially the if target signal's frequency is high. For the signals that are nonperiodic signals, the Fourier integral yields a continuous spectrum [56], and the result of the Fourier transform will provide a continuous spectrum. In the application of the analysis of noisy leakage current from the insulation structure's ground wire and the associated electric field around the structure, the main interest is in its frequency content and its associated amplitude.

The standard Fourier Transform is shown:

$$X(f) = \int_{-\infty}^{+\infty} x(t) e^{-j2\pi ft} dt \tag{A.4}$$

This function provides a representation of the frequency content of f, however ,it does not contain time-localization information, e.g. high-frequency oscillation due to partial discharge. In other words, the Fourier spectrum analysis is global in time and it is not the best tool for analyzing our target signals. Stationary signals are defined as the signal's properties that do not change during the analysis period. To analyze current from the insulation structure's ground wire, we which assume to be non-stationary and fast varying transient signals, Short Time Fourier Transform (STFT) - also called the Gabor transform - is introduced to improve the drawback of the Fourier analysis for nonstationary and fast transient signals [56, 60].

The main idea of STFT is to perform a time-dependent spectral analysis. The first step

is to divide the target non-stationary signals into a sequence of time segments where the signal may be considered as quasistationary [61]. The sequence of time segments is called the window, and in STFT the window's width is always fixed. Finally, the Fourier transform is applied to those individual signal segments. In 1946, Gabor was the first to introduce the short-time Fourier transform, known as the sliding window Fourier transform [56, 61]. The transform is defined as:

$$\mathrm{STFT}(\tau, f) = \int x(t) g^*(t-\tau) e^{-j2\pi f t} dt \tag{A.5}$$

where $g(t)$ is a square-integrable short-time window that has a fixed width and is shifted along the time axis by a factor $/tau$ [60]. Since the outcome of STFT is multiplied by the result of the Fourier transform on a sliding window that localizes the signal in the time domain, there is a convolution between the signal spectrum and the window spectrum. The narrower window we choose, the better we can localize the signal spectrum in the time domain. However, the window spectrum results get poorer. The width Δt of the window $g(t)$ in the time domain with the bandwidth Δf of the window $G(\Delta f)$ in frequency domain are defined respectively as:

$$\Delta t^2 = \frac{\int t^2 |g(t)|^2 dt}{\int |g(t)|^2 dt} \quad \Delta f^2 = \frac{\int t^2 |G(f)|^2 df}{\int |G(f)|^2 df} \tag{A.6}$$

where the denominator is the energy of the window in the time and frequency domains [60]. Δf is the resolution in the frequency domain of the short-time Fourier transform. It means that in the frequency domain, we need two signals' frequency at least more than Δf apart to make an identification [56]. Similarly, Δt is the resolution in the time domain. It means we need at least Δt second to discriminate two pulses in the time domain. Note that the STFT is a fixed window Fourier transform, that once a window has been selected, the two parameters given by Eq. A.6 will be fixed over the entire time-frequency plane.

The joint representation of time - frequency has an inherent limitation, and the resolutions are

limited by the principle:

$$\Delta t \Delta f \geq \frac{1}{4\pi} \tag{A.7}$$

This is also known as the Heisenberg inequality [61], one that is widely mentioned in quantum mechanics and important for time-frequency joint representation [56]. This principle points out that we cannot present a signal as a point in the time-frequency domain, we can only determine its position within a rectangle of $\Delta t \Delta f$ in the time-frequency space.

Since the time-bandwidth product $\Delta t \Delta f$ must follow this principle, it is necessary to choose our resolution parameters Δt and Δf wisely. In order to achieve the best resolution, we can only trade time resolution for frequency resolution or the other way around. Gabor proposed a solution to find Δt and Δf; he used a Gaussian function to represent the window function. The Fourier transform of the Gaussian window is still a Gaussian as

$$g(t) = \frac{1}{\sqrt{2\pi}s} e^{-\frac{t^2}{2s^2}} \text{ and } G(f) = e^{-\frac{s^2 \cdot (2\pi f)^2}{2}} \tag{A.8}$$

This Gaussian function also follows the uncertainty principle A.7 [56]. By applying the Gaussian function into Eq. A.3 we can get:

$$\Delta t^2 = \frac{s^2}{2} \text{ and } \Delta f^2 = \frac{1}{s^2 (2\pi)^2} \tag{A.9}$$

These two equations also satisfy the uncertainty principle A.7 and achieve the minimum time-bandwidth product $\Delta t \Delta f = \frac{1}{4\pi}$ [56].

We can conclude that the short-time Fourier analysis is good at processing non-stationary and fast varying transient signals. However, the analytical result is critically dependen on window selection. Thus, before using STFT, priori information concerning the time evaluation of the signal properties is required in order to make a priori choice of the window function [56, 60, 61].

Fig. A.3: Parallel plate electric field sensor used for PD detection.

A.3 Parallel Plate Electric Field Sensor

A parallel plate electric field sensor was used in this thesis for detection partial discharge activities in the air which is shown in Figure A.3. Basically, the parallel plate electric field sensor is a parallel plate capacitor. When the plate is placed in a changing electric field environment, a varies voltage will be induced between the two metal plates. The equivalent circuit is shown in Figure A.4.

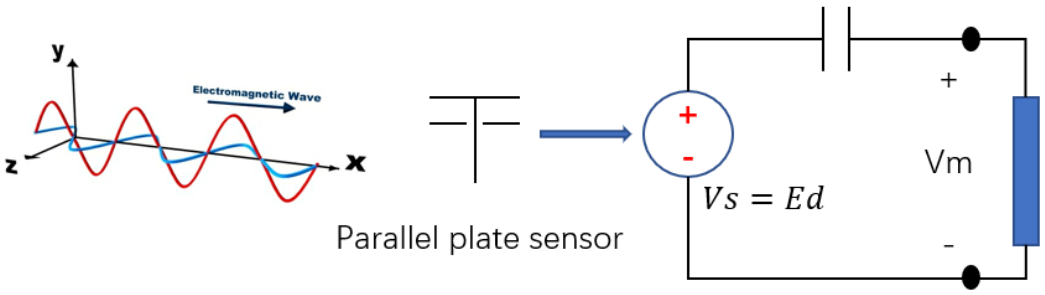

Fig. A.4: Equivalent circuit of parallel plate electric field sensor.

The measured voltage V_m at load end equals to:

$$V_m = \frac{R}{R + \frac{1}{j\omega C}} \times Ed \tag{A.10}$$

where E is the electric field in the environment, d is the distance between the parallel plate, and C is the capacitance of the parallel plate. When the electric field's frequency is low, the measured voltage V_m equals to:

$$V_m = j\omega C \times Ed \tag{A.11}$$

which will leads V_m to a negligible value. That is also why the parallel plate electric field sensor can only detect high frequency electric field signals.